NEUTRON DIFFUSION IN A SUBCRITICAL ASSEMBLY WITH SINUSOIDAL SOURCE OSCILLATION

ROBERT WILHELM CARIUS

NEUTRON DIFFUSION IN A SUBCRITICAL ASSEMBLY WITH SINUSOIDAL SOURCE OSCILLATION

by

Robert Wilhelm Carius

A Thesis Submitted to the
Graduate Faculty in Partial Fulfillment of
The Requirements for the Degree of
MASTER OF SCIENCE

Major Subject: Nuclear Engineering

Approved:

TABLE OF CONTENTS

I.	INTRODUCTION	1
II.	REVIEW OF THE LITERATURE	3
III.	LIST OF SYMBOLS	6
IV.	THEORETICAL ANALYSIS	8
	A. Transfer Function	8
	B. Attenuation Length of Neutron Wave	16
V.	EXPERIMENTAL EQUIPMENT	18
	A. Subcritical Assembly	18
	B. Oscillator Unit	22
	C. Counting Apparatus	25
VI.	EXPERIMENTAL PROCEDURE	29
	A. Description of Typical Run	29
	B. Determination of Phase Angle	31
	C. Determination of γ by Amplitude Ratios	34
	D. Determination of γ by Median-flux Levels	35
	E. Determination of Amplitude Ratio	35
	F. Determination of Median-flux Level	37
VII.	RESULTS	38
VIII.	DISCUSSION OF RESULTS	48
IX.	CONCLUSIONS	62
X.	SUGGESTIONS FOR FURTHER STUDY	64
XI.	LITERATURE CITED	66
XII.	ACKNOWLEDGMENTS	68
XIII.	APPENDIX	69

I. INTRODUCTION

The subcritical assembly initially was utilized as an experimental unit to determine if a chain-reacting assembly were possible. As reactor technology progressed the assembly came to be used more and more as a test unit for proposed reactor designs and materials, and the majority of these test investigations have been conducted in the steady or equilibrium state. Operation of the assembly by disturbance of the steady state has led to new areas of investigation.

Frequent utilization of the subcritical assembly as a test unit has come about naturally. Cost of a subcritical assembly is considerably lower than that for a critical assembly since special safety equipment is not needed (11, p. 103). Less fuel and moderator are used, and experiments can be conducted easier in the subcritical than in the critical assembly.

Disturbance of the steady state may be accomplished by two methods, reactivity forcing and source forcing. Reactivity forcing can be represented as a change in the neutron density brought about by a small harmonic variation in the reactivity, whereas source forcing is produced by a variation in the rate at which neutrons are being added to the assembly.

Thus far the investigation of the dynamic response of a system has been limited to servomechanism theory, which treats the system as a "black box". Phase and amplitude

response of the system in relation to a forcing function must be determined in order to apply servomechanism theory. The above relationship called the transfer function is derived by noting the responses as indicated brought about by either reactivity or source forcing.

It is believed however that neutron diffusion in a subcritical assembly will not produce identical phase and amplitude responses throughout. These variations should depend upon the method of varying the rate of neutrons from the source and the position of neutron-flux measurement.

The purpose of this investigation was threefold. First, an experimental verification of the theoretical transfer function for a subcritical assembly was attempted using a varying rate of neutrons from the source. Secondly, neutron diffusion in the subcritical assembly that shows variance from the predicted identical phase and amplitude response throughout the assembly was investigated. The last area of investigation was an attempt to determine assembly characteristics by using a sinusoidally varying source.

II. REVIEW OF THE LITERATURE

A reasonable amount of literature is available on the development and usage of the transfer function of a critical assembly. Original work in the field was carried out by Owens, Crever and Pigott (12) in 1949, in which an automatic control unit was used to compensate for reactivity variations in order to maintain the desired power level in a reactor. Their work showed that the assembly transfer function exhibited proper characteristics to describe the reactivity variations in the assembly.

Later that same year, Franz (4) developed the general form of the transfer function of a nuclear reactor by applying the standard techniques of servo theory. He applied the transfer function to an electronic assembly simulator to predict assembly response to a step-function change of reactivity.

The practical verification of using a subcritical assembly in testing reactor components was shown by Axtmann, Dessauer, and Parkinson (1) in 1955. A chain-reacting "test assembly" was utilized to test materials by noting effects on the kinetic behavior of the assembly. Identical tests were conducted in a subcritical assembly, and the results were nearly identical with the subcritical assembly producing results faster, cheaper and safer.

Glasstone (5) briefly discussed the transfer function in a subcritical assembly. In his development he assumed a sinusoidal variation in source strength and used electrical analogs of reactor quantities to indicate the relationship of electrical parameters with the reactor parameters, reactivity forcing and source forcing.

Weinberg and Schweinler (15) developed the equations for the response of a critical chain-reacting assembly to a thermal neutron absorber which is oscillated back and forth inside the assembly. They further stated that at frequencies which are low compared to the reciprocal periods of the delayed neutrons, the neutron density in the assembly rises and falls as a whole. However, if the frequency is much greater than the reciprocal period of the delayed neutrons, a spherical neutron wave emanates from the vicinity of the oscillator and is attenuated in an exponential manner with distance as it is propagated.

Weinberg and Wigner (16) extended this theory to subcritical assemblies. It was stated that the neutron-wave wave length is related to the material buckling. They suggested that the exponential-experiment method of determining material buckling could be performed by measuring the properties of neutron waves established by a localized oscillating neutron source. A particularly desirable feature of this method is that an experiment to determine material

buckling can be performed in an assembly of smaller dimensions than that required by the normal exponential experiment.

III. LIST OF SYMBOLS

A	Activity	counts/min.
a	Width of assembly	in.
a.l.	Attenuation length	in., cm.
B^2	Buckling	$cm.^{-2}$
β	Fraction of average group of delayed neutrons	
β_i	Fraction of i^{th} group of delayed neutrons	
C	Concentration of average group of delayed neutron precursors	
C_e	End-correction factor	
C_h	Harmonic-correction factor	
C_i	Concentration of i^{th} group of delayed neutron precursors	
D	Thermal neutron diffusion coefficient	cm.
f	Thermal utilization	
γ	Inverse relaxation length	$in.^{-1}$
j	$\sqrt{-1}$	
K	Constant	
k	Effective multiplication factor	
k_∞	Multiplication factor for an infinite assembly	
L	Neutron diffusion length in assembly	cm.
ℓ	Average neutron lifetime in a finite assembly	sec.
ℓ_o	Mean neutron lifetime in an infinite assembly	sec.

λ	Decay constant of average group of delayed neutron precursors	$sec.^{-1}$
λ_1	Decay constant of the i^{th} group of delayed neutron precursors	$sec.^{-1}$
M^2	Migration area	$in.^2$, $cm.^2$
n	Number of neutrons of thermal energies	$neutrons/cm.^2$
ω	Frequency of oscillation	$\frac{radians}{sec.}$
p	Resonance escape probability	
ϕ	Thermal neutron flux	$\frac{neutrons}{cm.^2\ sec.}$
Σ	Macroscopic cross section	$in.^{-1}$, $cm.^{-1}$
t	Time	sec.
τ	Fermi age	$cm.^2$
v	Thermal neutron mean velocity	cm./sec.
z	Vertical distance above base of assembly	in.

Subscript:

a	Absorption
dn	Delayed neutron
e	External
g	Graphite
i	i^{th} part
mn	Harmonic mn
p	Prompt
o	Steady state
1	Complex amplitude
11,13,31,33	Harmonics of γ

IV. THEORETICAL ANALYSIS

A. Transfer Function

The transfer function is defined as the ratio of the phase and amplitude response to a sinusoidally-varying forcing function. This response for a subcritical assembly can be obtained from the time-dependent general diffusion equation. Thermal neutrons only will be considered since the experimental equipment is designed to vary the rate at which thermal neutrons enter the assembly. The basic equation is (6, p. 101)

$$D \nabla^2 \phi - \Sigma_a \phi + S = \frac{\partial n}{\partial t} = \frac{1}{v} \frac{\partial \phi}{\partial t} \qquad \text{Eq. 1}$$

where $\phi = n v$, and v is assumed to be constant.

The source term can be separated into three parts. The first term is due to the prompt neutrons resulting from fission. Fermi-age theory yields this part of the source term to be (5, p. 226)

$$S_p = (1 - \beta) k_\infty \Sigma_a \phi e^{-B^2 \tau} \qquad \text{Eq. 2}$$

where β is the fraction of all the delayed neutrons.

The second part of the source term is due to the delayed neutrons resulting from decay of various fission products. A total of six groups of delayed fission neutrons are utilized in expressing this part of the source term. Each

group has its own value of λ_i, β_i and C_i. The net rate of formation of the delayed-neutron precursors is then

$$\frac{\partial C_i}{\partial t} = \beta_i \frac{k_\infty}{p} \Sigma_a \phi - \lambda_i C_i \,. \qquad \text{Eq. 3}$$

The delayed-neutron source term using Fermi-age theory can be expressed as (5, p. 227)

$$S_{dn} = p\, e^{-B^2\tau} \sum_{i=1}^{6} \lambda_i C_i \qquad \text{Eq. 4}$$

where $\sum_{i=1}^{6} \lambda_i C_i$ is the decay rate of the precursor which is numerically equal to the rate of production of the delayed neutrons. The Fermi-age for the delayed neutrons has been taken equal to that of the prompt neutrons (5, p. 227).

The last part of the source term is due to the external source which in this analysis supplies the source forcing needed. It is written as

$$S_e = S_o + S_1 e^{j\omega t} \,. \qquad \text{Eq. 5}$$

With substitution of the above expressions of the source term into Equation 1 the following equation is obtained

$$D \nabla^2 \phi - \Sigma_a \phi + (1-\beta) k_\infty \Sigma_a \phi\, e^{-B^2\tau} + p\, e^{-B^2\tau} \sum_{i=1}^{6} \lambda_i C_i + S_o + S_1 e^{j\omega t} = \frac{1}{v} \frac{\partial \phi}{\partial t} \,. \qquad \text{Eq. 6}$$

The space and time variables are considered separable when k remains constant (5, p. 227). This yields an ordinary differential equation for Equation 6. If the subcritical system is large, then $\nabla^2 \phi = -B^2 \phi$ (6, p. 361).

Let $$\ell_o = \frac{1}{\Sigma_a v} \qquad \text{Eq. 7}$$

and $$L^2 = D/\Sigma_a \qquad \text{Eq. 8}$$

and divide Equation 6 through by Σ_a, to obtain the result

$$- (L^2B^2 + 1)\phi + (1 - \beta) k_\infty e^{-B^2\tau} \phi + \frac{p}{\Sigma_a} e^{-B^2\tau} \sum_{i=1}^{6} \lambda_i C_i + \frac{S_o}{\Sigma_a} + \frac{S_1 e^{j\omega t}}{\Sigma_a} = \ell_o \frac{d\phi}{dt} \quad . \qquad \text{Eq. 9}$$

With division of Equation 9 through by $(1 + L^2B^2)$ and the use of the relationships

$$k = \frac{k_\infty e^{-B^2\tau}}{1 + L^2B^2} \qquad \text{Eq. 10}$$

and

$$\ell = \frac{\ell_o}{1 + L^2B^2} \qquad \text{Eq. 11}$$

Equation 9 becomes

$$- \phi + (1 - \beta)\, k\, \phi + \frac{p}{\Sigma_a} \frac{k}{k_\infty} \sum_{i=1}^{6} \lambda_i C_i + \frac{S_o + S_1 e^{j\omega t}}{\Sigma_a (1 + L^2B^2)} = \ell \frac{d\phi}{dt} . \qquad \text{Eq. 12}$$

With division by ℓ, and utilization of $\phi = n v$, Equation 12 is reduced to

$$[k(1 - \beta) - 1] \frac{n v}{\ell} + \frac{p}{\Sigma_a} \frac{k}{\ell k_\infty} \sum_{i=1}^{6} \lambda_i C_i + \frac{S_o + S_1 e^{j\omega t}}{\Sigma_a \ell (1 + L^2B^2)} = v \frac{dn}{dt} . \qquad \text{Eq. 13}$$

With rearrangement Equations 10 and 11 become

$$\frac{k}{\ell k_\infty} = \frac{e^{-B^2\tau}}{\ell_o} = e^{-B^2\tau} \Sigma_a v \qquad \text{Eq. 14}$$

and

$$\ell_o = \ell(1 + L^2B^2) = \frac{1}{\Sigma_a v}$$

or

$$1/v = \Sigma_a \ell (1 + L^2B^2) . \qquad \text{Eq. 15}$$

Equation 13 with use of the above two substitutions and division through by v yields

$$[k(1 - \beta) - 1] \frac{n}{\ell} + p\, e^{-B^2\tau} \sum_{i=1}^{6} \lambda_i C_i + S_o + S_1 e^{j\omega t} = \frac{dn}{dt} . \qquad \text{Eq. 16}$$

In a similar manner, Equation 3 with the use of Equations 10 and 15 is found to be

$$\frac{d\,C_i}{d\,t} = \beta_i \frac{k\,n}{p\,\ell\,e^{-B^2\tau}} - \lambda_i\,C_i \quad . \qquad \text{Eq. 17}$$

Solving for $\lambda_i\,C_i$ and substituting into Equation 16 yields

$$[k(1-\beta)-1]\frac{n}{\ell} + p\,e^{-B^2\tau}\sum_{i=1}^{6}\left[\frac{\beta_i\,k\,n}{p\,e^{-B^2\tau}\,\ell} - \frac{d\,C_i}{d\,t}\right] + S_o + S_1\,e^{j\omega t} = \frac{d\,n}{d\,t} \qquad \text{Eq. 18}$$

or

$$\frac{d\,n}{d\,t} = (k-1)\frac{n}{\ell} - p\,e^{-B^2\tau}\sum_{i=1}^{6}\frac{d\,C_i}{d\,t} + S_o + S_1\,e^{j\omega t} \qquad \text{Eq. 19}$$

since

$$\sum_{i=1}^{6}\frac{\beta_i\,k\,n}{\ell} = \frac{\beta\,k\,n}{\ell} \quad .$$

Solving this for n gives

$$n = \frac{\ell}{(k-1)}\left[p\,e^{-B^2\tau}\sum_{i=1}^{6}\frac{d\,C_i}{d\,t} + \frac{d\,n}{d\,t}\right] + \frac{\ell\,(S_o + S_1\,e^{j\omega t})}{(1-k)} \quad . \qquad \text{Eq. 20}$$

In this particular case the value of k will remain constant. Neither assembly geometry nor fuel-loading changes will take place in the experiment. However both the neutron density and precursor concentration will vary as

$$n = n_o + n_1 e^{j\omega t} \qquad \text{Eq. 21}$$

and

$$C_i = C_{oi} + C_{1i} e^{j\omega t} \qquad \text{Eq. 22}$$

where n_1 and C_1 are the complex amplitudes. With the aid of Equations 17, 21 and 22, Equation 20 yields

$$n_o + n_1 e^{j\omega t} = \frac{\ell}{(k-1)} \left[p\, e^{-B^2\tau} \sum_{i=1}^{6} \left\{ \frac{\beta_i k}{\ell\, p\, e^{-B^2\tau}} (n_o + n_1 e^{j\omega t}) - \lambda_i (C_{oi} + C_{1i} e^{j\omega t}) \right\} + \frac{d}{dt}(n_o + n_1 e^{j\omega t}) \right] + \frac{\ell (S_o + S_1 e^{j\omega t})}{(1-k)} . \qquad \text{Eq. 23}$$

The complete solution to Equation 23 involves using the six groups of delayed neutrons each with its discrete value of λ_i, β_i, and C_i. The solution using an average group of delayed neutrons will be shown.

Equation 23 can be separated into steady and sinusoidal components, and each constitutes a valid equality. The

transfer function uses only the sinusoidal component, which with group notation eliminated, is

$$n_1 e^{j\omega t} = \frac{\ell}{(k-1)}\left[\frac{\beta k}{\ell} n_1 e^{j\omega t} - p e^{-B^2\tau}\lambda C_1 e^{j\omega t} + \frac{d}{dt}(n_1 e^{j\omega t})\right] + \frac{\ell S_1 e^{j\omega t}}{(1-k)} \quad . \qquad \text{Eq. 24}$$

Again using Equation 17 and substituting Equations 21 and 22 gives

$$\frac{k\beta}{p e^{-B^2\tau}\ell}(n_o + n_1 e^{j\omega t}) = \lambda(C_o + C_1 e^{j\omega t}) + \frac{d}{dt}(C_o + C_1 e^{j\omega t}) \quad . \qquad \text{Eq. 25}$$

The sinusoidal portion of which becomes

$$\frac{k\beta}{p\ell e^{-B^2\tau}} n_1 e^{j\omega t} = \lambda C_1 e^{j\omega t} + j\omega C_1 e^{j\omega t} \quad , \qquad \text{Eq. 26}$$

which reduces to

$$\frac{\beta k n_1}{(\lambda + j\omega) C_1} = p\ell e^{-B^2\tau} \quad . \qquad \text{Eq. 27}$$

Substituting Equation 27 into Equation 24 yields

$$n_1 e^{j\omega t} = \frac{\beta k n_1 e^{j\omega t}}{(k-1)} - \frac{\lambda C_1 e^{j\omega t}}{(k-1)}$$

$$\left[\frac{\beta k n_1}{(\lambda + j\omega) C_1}\right] + \frac{\ell j\omega n_1 e^{j\omega t}}{(k-1)}$$

$$+ \frac{\ell S_1 e^{j\omega t}}{(1-k)} \quad . \qquad \text{Eq. 28}$$

By definition, the amplitude portion of the transfer function is the ratio of the response to the sinusoidally - varying driving source. The ratio can be expressed as

$$\frac{n_1}{S_1}\left[\frac{1-k}{\ell}\right] \qquad \text{Eq. 29}$$

or from Equation 28

$$\frac{n_1}{S_1}\left[\frac{1-k}{\ell}\right]$$

$$= \frac{1}{\left[1 + \frac{\beta k}{(1-k)} - \frac{\lambda k \beta}{(\lambda + j\omega)(1-k)} + \frac{\ell j\omega}{(1-k)}\right]} \quad . \qquad \text{Eq. 30}$$

Rearranging Equation 30 by putting the right side denominator under the common factor $(\lambda + j\omega)(1-k)$, multiplying through by $\lambda + j\omega$, then dividing by λ and simplifying gives the desired form

$$\frac{n_1}{S_1}\left[\frac{1-k}{\ell}\right] = \frac{1 + \frac{j\omega}{\lambda}}{1 - \frac{\omega^2 \ell}{\lambda(1-k)} + \frac{j\omega}{\lambda}\left[1 + \frac{\lambda\ell + \beta k}{(1-k)}\right]} \cdot \qquad \text{Eq. 31}$$

B. Attenuation Length of Neutron Wave

When the rate at which neutrons entering a subcritical assembly is oscillated in a sinusoidal manner at a frequency considerably greater than the reciprocal period of the delayed neutrons a neutron wave is propagated. With an average delayed neutron period of approximately 10 seconds, frequencies greater than one radian/second should produce these neutron waves. Frequencies considerably less than the delayed-neutron reciprocal period allow the delayed neutrons to remain in equilibrium with the prompt neutrons (14, p. 100). However, at higher frequencies the assembly behaves as if there were no delayed neutrons and the delayed neutrons merely contribute to the background. Hence the neutron wave has characteristics that are dependent upon the "prompt" response of the assembly. These characteristics, wave length, velocity, and attenuation length are all dependent upon the frequency of oscillation.

Weinberg and Wigner (16, p. 437) developed equations for the three neutron-wave characteristics. The equation

for the characteristic that is of importance here, attenuation length, is

$$\text{a.l.} = \frac{\sqrt{2M}}{\left\{\left[(k_p - 1)^2 + (\omega \ell_o)^2\right]^{1/2} - (k_p - 1)\right\}^{1/2}} \qquad \text{Eq. 32}$$

where ω is greater than one radian/second. Attenuation length is defined as the distance for wave amplitude to decrease by a factor of e.

If a neutron wave were propagated by using a high-frequency sinusoidal source oscillation then attenuation length could be determined. Amplitudes of the sine wave in selected vertical positions could be measured, and a value for attenuation length would then be determined from the equation $A = K\, e^{-z/a.l.}$, where A is the amplitude at z, and K is a constant. A semi-log plot of amplitude versus vertical position will yield a slope of 1/a.l. This value of 1/a.l. is the "inverse relaxation length" of the complex buckling for the frequency investigated. If the phase angle is small at a given frequency, the attenuation length at that frequency would be approximately equal to relaxation length used to calculate material buckling. Therefore, the complex buckling determined by this value of attenuation length would be approximately equal to the material buckling.

V. EXPERIMENTAL EQUIPMENT

A. Subcritical Assembly

The subcritical assembly used for the experimental investigation is shown in Figure 1 with the east cover removed. Cylindrical rods of graphite measuring 7 inches in diameter were machined to a square from 6 inches across, leaving rounded corners. These blocks of AGR-grade graphite were then stacked in ten columns nine rows high to form the lower section of the assembly. For the top five rows cylindrical graphite rods 6-3/8 inches in diameter were machined to a 5 inch by 6 inch cross section with rounded corners. The space available between the corners of adjoining blocks was utilized for insertion of fuel elements or measuring equipment.

The graphite blocks were assembled upon a plywood sheet supported by a wooden pedestal. As shown in Figure 1, the pedestal was divided into three accessible spaces approximately one foot high. The two outermost spaces contained open-topped aluminum tanks, filled with water, which extended the width of the assembly. They served to moderate the neutrons and to reduce radiations coming directly from the sources located in the oscillator unit beneath the assembly. Figure 2 shows the oscillator unit and selective-count device which was placed in the center access section

Figure 1. The subcritical assembly

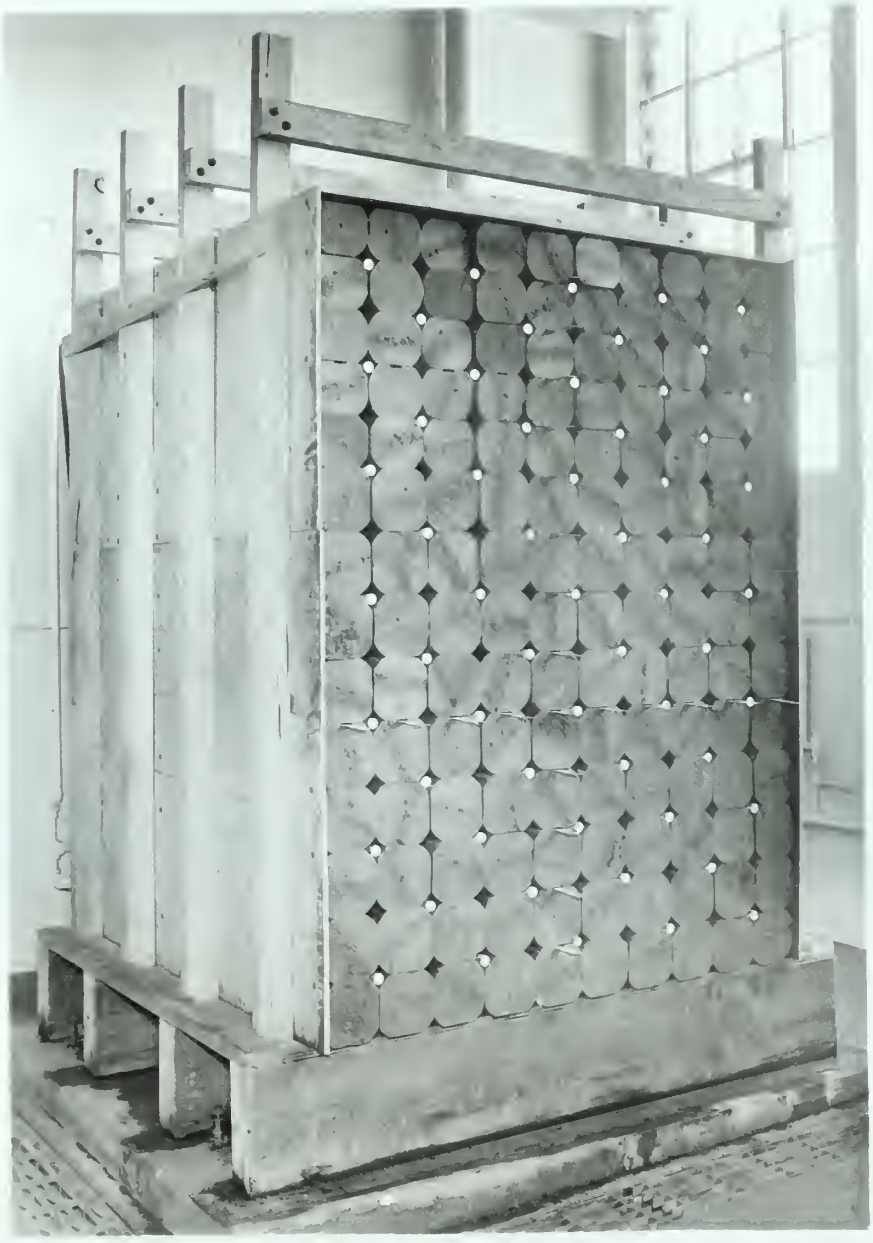

Figure 2. The oscillator unit and selective-count device

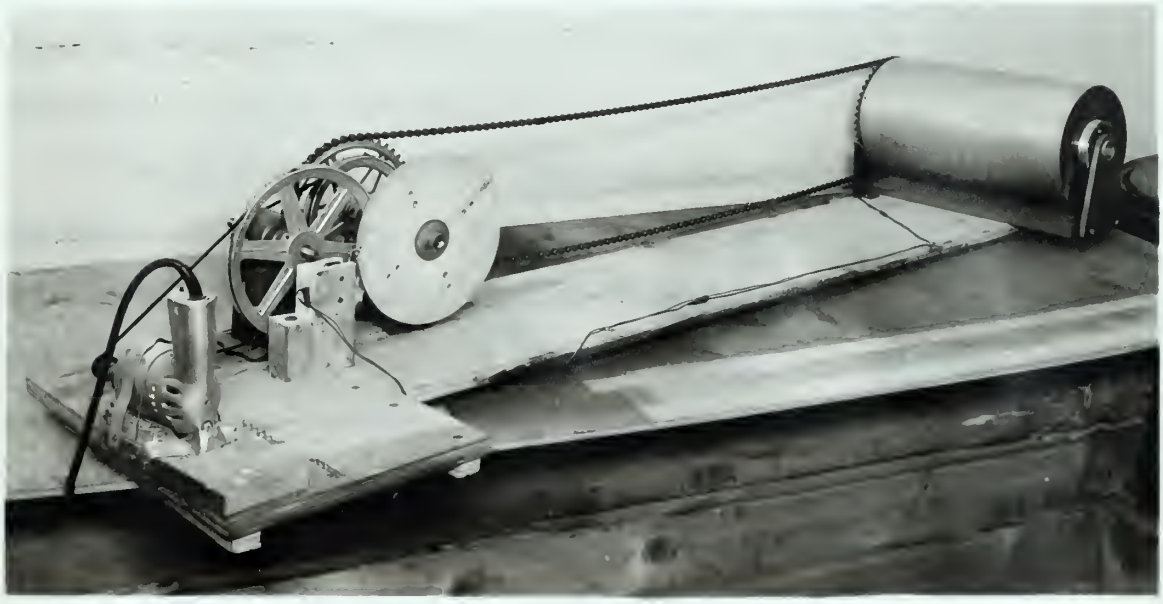

beneath the assembly.

All four sides and top of the assembled graphite were covered with 10-mil cadmium sandwiched between a 0.375-inch thickness of plywood and 0.125 inches of masonite. Approximately 95 percent of all thermal neutrons were stopped by this cadmium sheet, giving a "black boundary" to thermal neutrons. A wooden framework braced the north and south sides of the assembly and both the east and west faces were removable for easy access.

Natural uranium in the form of cylindrical rods 1.0 inches in diameter and 8.0 inches long served as the fuel. These rods were encased by 2S aluminum cans with a 0.040-inch wall thickness and end caps 0.200 inches thick. Each can of uranium was then helically wound with a spacing wire and placed into a 61S aluminum tube, 62 inches long with an outside diameter of 1.375 inches and a wall thickness of 0.035 inches. Approximately 10 feet of the 2S-aluminum spacing wire was needed for each tube. A total of seven canned uranium rods were placed in each tube to constitute one fuel element. With the fuel elements placed in every other hole as shown in Figure 1 an 8.5-inch square lattice in the lower region of the assembly was formed. This lattice configuration was maintained throughout the experimental investigation.

B. Oscillator Unit

The oscillator unit and selective-count device is shown in Figure 2. The drum-type assembly at the right end is the oscillator unit itself and is shown schematically in Figure 3. This unit was designed to contain the five one-curie Pu-Be sources and to vary the rate at which thermal neutrons were emitted from the source in a sinusoidal manner.

Each cylindrical source measuring 1 inch in diameter and 1-3/8 inches high was placed in the source retainer. A non-rotating-paraffin jacket surrounding the retainer was constructed of 1/16-inch aluminum sheet rolled into a diameter of 7-3/8 inches. End caps of 1/8-inch aluminum were attached, giving an overall length of 14.5 inches. Twenty-five pounds of white paraffin were poured into the jacket through a filler cap, and precautions were taken to reduce the possibility of shrinkage voids. Moderation to supply the thermal neutrons desired was provided by the three inches of paraffin. The paraffin jacket and the bearings for the pattern cylinder were both supported by the source retainer which extended to the support brackets.

An outer rotating cylinder, the pattern cylinder, was also formed from 1/8-inch aluminum sheet. Its dimensions were an outside diameter of 8 inches and a length of 15

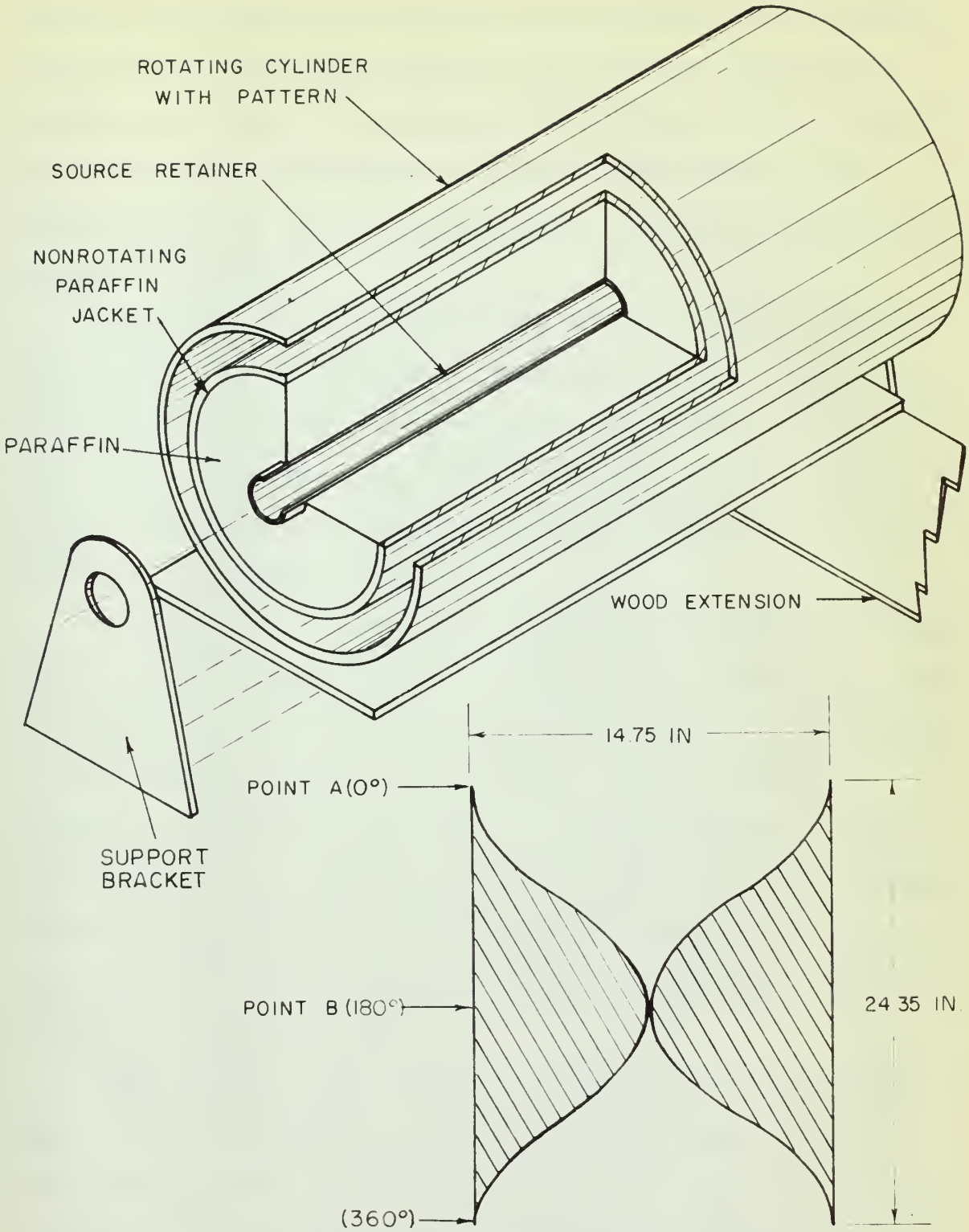

Figure 3. Oscillator unit and cadmium-pattern detail

inches. End plates made from 1/4-inch aluminum were fitted and screwed to a collar fitted on its bearing outer-run casing. The inner-run casing of the bearing rested on the source retainer for support. To give easy access to the inner section of the pattern cylinder the end plates were attached by screws.

A sine pattern with the dimensions as shown in Figure 3 was cut from 10-mil cadmium. Three thicknesses, giving a total of 0.030 inches, were cemented to the inner surface of the pattern cylinder. Most of the thermal neutrons were stopped and a small fraction of the fast attenuated by this thickness of cadmium (10, p. 12).

Point A of the pattern was the wide-open position, allowing the maximum number of thermal neutrons to escape from the oscillator unit. The closed position, point B, stopped most of the thermal neutrons. When point A was at top-dead center, the oscillator unit was at the zero-degree position. The 180-degree position occurred when point B was at top-dead center. Hence the exact position of the sine pattern of the oscillator unit was designated by a given angle from 0 to 360 oscillator degrees.

Measurements taken within 1.5 inches of the oscillator unit at the two extreme positions described above showed that the paraffin jacket moderated a satisfactory percentage of neutrons to be used in the experimental investigation.

The value obtained at position A minus that at B was 58 percent of the value at position A.

C. Counting Apparatus

In order to measure the neutron flux during a designated number of oscillator-unit degrees a selective-count device was constructed. A positive, non-slip linkage had to be supplied from the oscillator unit to a position removed from the neutron sources. The equipment needed to select the number of oscillator degrees in which counting would take place was located at this "removed" position.

A bicycle sprocket was bolted to the end plate of the pattern cylinder. A 110-inch bicycle chain was used to connect this sprocket on the oscillator unit to a sprocket of the same diameter mounted on a countershaft at the removed position. Position by degrees of the oscillator unit was then transmitted unchanged to the "removed" position where work could be performed without the intense radiation.

The countershaft was a polishing-head spindle which was mounted on a 3/4-inch plywood extension connecting the oscillator unit to the remainder of the equipment. At one end of the spindle shaft a 6-inch V-belt pulley was locked to the shaft, and the bicycle sprocket was in turn bolted to this pulley. At the opposite end of the shaft was locked a plywood plate, 6-3/4 inches in diameter. The polishing-

head spindle was driven by a 1/4-inch Black and Decker electric drill connected to it by a leather belt. Rotation frequency was controlled by varying the voltage to the drill. In order to improve the frequency control at slow speeds (below 50 RPM) a second polishing-head spindle was interposed as shown in Figure 2. These two configurations then gave a speed range for the oscillator unit of from 4 to 1000 RPM.

A 1/4-inch plywood plate of 8.14-inches diameter with a 30-degree cam hump was fabricated. To prevent wear a metal strip was cemented to the cam. A similar 10-degree cam was also constructed. The cam, with a 1/2-inch centering hole, was held securely by a nut against the plywood plate on the spindle shaft. A compass card oriented to the exact oscillator degree was secured to this plywood plate. The cam was set at any desired oscillator position by loosening the cam-holding nut.

As shown in Figure 2 a microswitch was positioned adjacent to the cam. The switch was wired in the normally-open position to the preset-time relay of a Radiation Instrument Development Laboratories, model 206, scaler. The cam was positioned by use of the compass card to make contact with the switch at a specified oscillator degree. When the sine pattern of the oscillator unit reached this degree the cam made contact and the switch was closed. This closed the preset-time relay allowing the scaler to begin to count.

When the microswitch broke contact the relay of the scaler opened, ceasing the count.

A Radiation Counter Laboratories boron trifloride proportional counter, model 10503, was inserted midway into the assembly through holes cut into the east cover. It in turn was connected to the Radiation Instrument Development Laboratories scaler.

The oscillator unit and selective-count device was inserted from the south end of the assembly until the oscillator unit was at the center. As shown in Figure 4 this placed only the oscillator unit itself beneath the assembly; the remaining equipment was outside to facilitate changing the cam setting.

Figure 4. Experimental set up

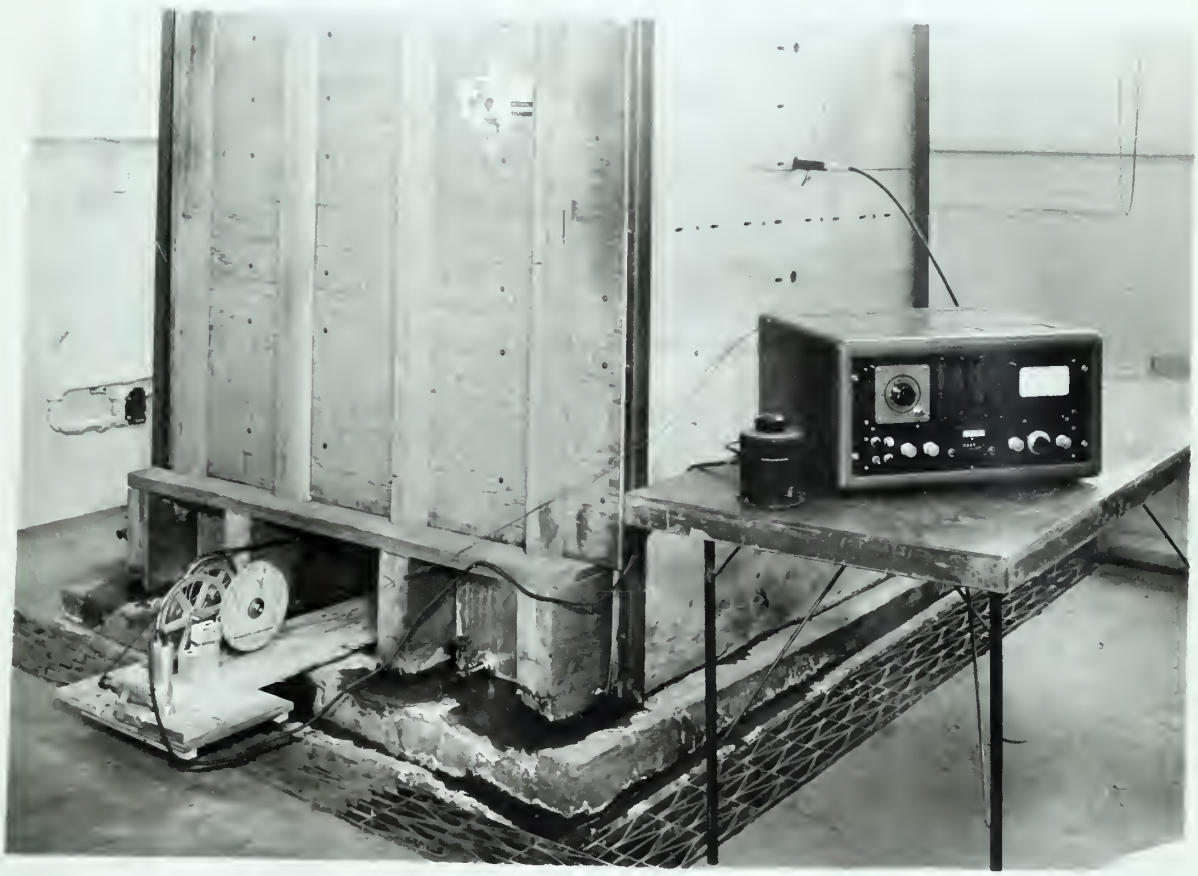

VI. EXPERIMENTAL PROCEDURE

A. Description of Typical Run

The fuel elements were loaded into the assembly as shown in Figure 1. Measurements were taken only in the center of the assembly. Holes drilled on the east-cover centerline matched assembly holes between the graphite blocks. The holes were one foot, two feet, three feet, four feet and four feet eleven inches above the base. Hereafter these holes will be referred to as holes one through five respectively.

The neutron detector was inserted midway into the assembly and the oscillator unit set at 0 degrees. With the 30-degree cam set at a mean position of 0 degrees, initial contact with the microswitch was made at 345 degrees.

Oscillator speed was adjusted to the desired RPM by referring to a stop watch and counting revolutions. When desired speed was obtained the watch was started and the preset-time switch on the scaler was actuated. Runs varied in duration from one to five minutes depending on position and oscillator speed. A run was completed when a designated number of counting periods had elapsed rather than ending at an exact time interval. For example, a run for 3 minutes at 18 RPM requires 54 counting periods; when 54 periods had elapsed the preset-count switch was turned off even though

the time may have been a few seconds on either side of 3 minutes. It was difficult to control the speed exactly and this procedure eliminated varying numbers of counting periods in a single series of runs.

The counts were recorded from the scaler; the drill turned off; the cam reset to a mean position of 30 degrees and the entire counting procedure repeated. The counting procedure continued in 30-degree increments until the entire 360 degrees had been surveyed yielding one single series of runs.

Speeds (frequency of oscillation) used in the investigation were selected at regular intervals on a logarithmic scale. Runs were attempted throughout the entire range of the equipment. The lowest constant speed attainable was 4 RPM. An upper limit on speed was imposed by the cam and microswitch arrangement, for in speeds beyond 180 RPM the switch hammered the cam as the switch spring forced the idler back to the surface of the cam. As runs were made in the higher hole positions at high speeds the data became unusable. This was caused by the exponential attenuation of neutron flux up the assembly and a consequently smaller difference from the highest to the lowest count rate in a series of runs. When this occurred the counting rates when plotted against degrees did not yield a satisfactory distribution.

Original data for the various runs completed is shown in Tables 5 through 12 in the Appendix.

B. Determination of Phase Angle

The count rates for a single series of runs were plotted on graph paper. Standard deviation for each point was also plotted to facilitate drawing a representative curve through the points. All the plots that showed a trend in distribution gave a sinusoidal result. Figure 5 shows a plot of the data for all holes at 2.51 radians/second, and as mentioned previously some unusable data was taken and the basis for declaring it unusable was large scatter in the plotted curves.

From the general trend of the plot and especially from the position of the highest and lowest counting rates the phase angle for that series of runs was determined. To ensure that an accurate phase angle was being obtained a 10-degree cam was utilized. Five-minute counts were taken every ten degrees in the region of the maximum counting rate, however use of the 10-degree cam was restricted to the lower speeds.

It was assumed in determining the phase angle that the oscillator unit when in the 0-degree position during rotation and the counting equipment would yield the highest counting rate. To validate this assumption an entire series of calibration runs with the neutron detector held 1.5 inches from the oscillator unit in position beneath the assembly was made. Table 13 in the Appendix and Figure 5

Figure 5. Plots of typical data

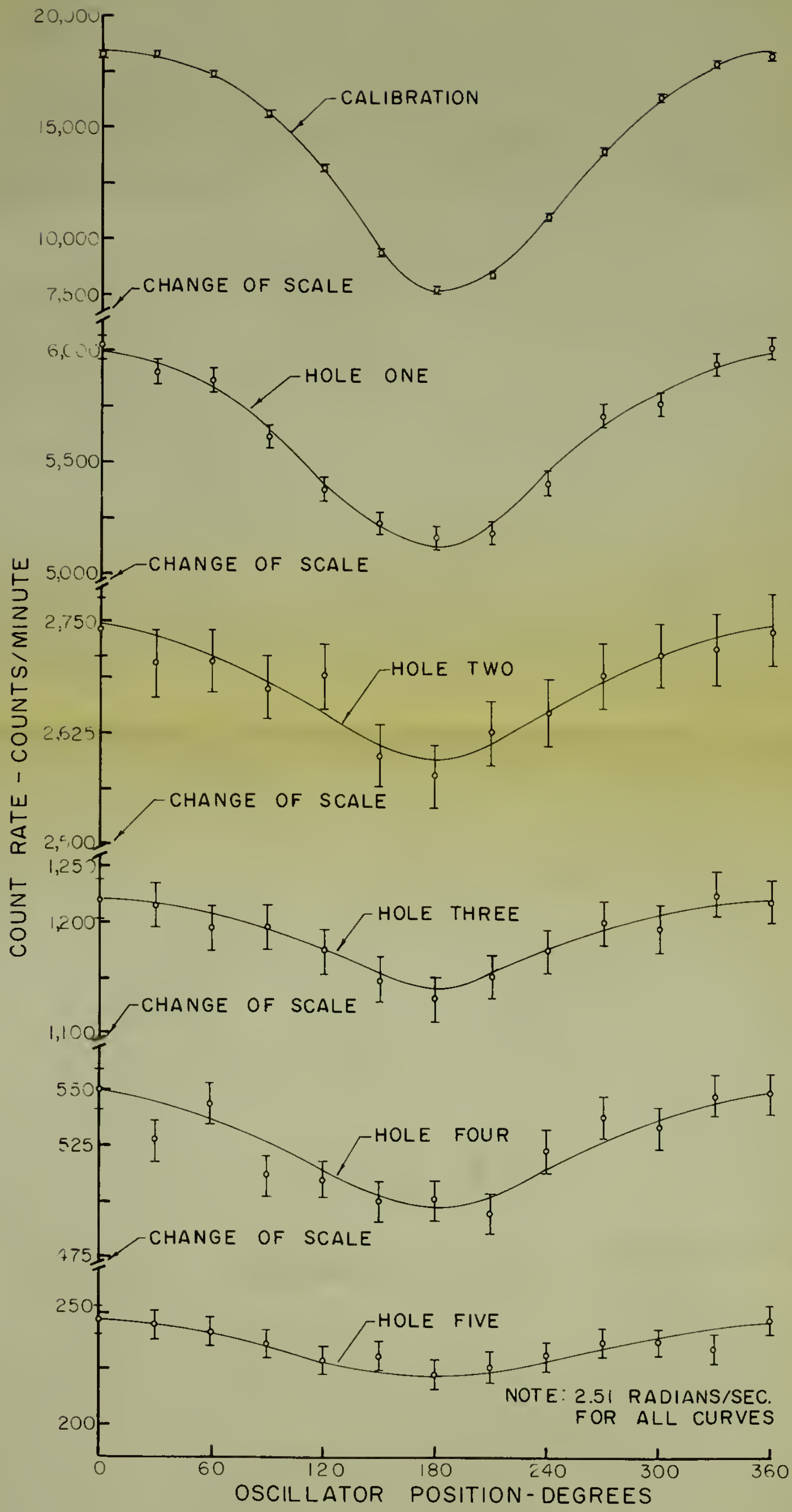
COUNT RATE - COUNTS/MINUTE
20,000
15,000
10,000
7,500
CHANGE OF SCALE
CALIBRATION
6,000
5,500
5,000
CHANGE OF SCALE
HOLE ONE
2,750
2,625
2,500
CHANGE OF SCALE
HOLE TWO
1,250
1,200
1,100
CHANGE OF SCALE
HOLE THREE
550
525
475
CHANGE OF SCALE
HOLE FOUR
250
200
HOLE FIVE
NOTE: 2.51 RADIANS/SEC.
FOR ALL CURVES
0
60
120
180
240
300
360
OSCILLATOR POSITION - DEGREES

indicate the results which show that there was no "built in" phase angle.

C. Determination of γ by Amplitude Ratios

The inverse relaxation length for the thermal-neutron flux in the assembly, γ , was determined by amplitude ratios for various frequencies of oscillation. The value actually obtained was the inverse attenuation length, but as previously noted, under certain conditions these values are approximately equal. The experimental conditions were such that the above statement is true, and will be demonstrated in the Discussion of Results.

Uncorrected-amplitude ratios were used in place of foil activities in the equation $A = Ce^{-\gamma z}$. With the method of least squares an initial uncorrected value for γ was found (2, p. 166). Both end-correction and harmonic-correction factors* were determined and applied to the amplitude ratios

---

*End-correction factor: $C_e = 1 - e^{-2\gamma_{11}(c-z)}$

Harmonic-correction factor: $C_h = 1 + \gamma_{11} e^{\gamma_{11} z}$

$$\left[\frac{1}{\gamma_{13}} e^{-\gamma_{13} z} + \frac{1}{\gamma_{31}} e^{-\gamma_{31} z} + \frac{1}{\gamma_{33}} e^{-\gamma_{33} z} \right]$$

where $\gamma_{mn}^2 = (\pi/a)^2 (m^2 + n^2 - 2) + \gamma_{11}^2$.

with this initial value of γ. The origin of the Z-axis was taken at the base of the assembly; therefore hole one was at a position of z = 12 inches. A second value for γ was determined with the corrected amplitude ratios. This process was repeated until the value of γ used in the correction factors agreed with the γ found by using the corrected amplitude ratios. Computations showed that harmonic corrections were significant only for the three lower holes and end corrections for the two upper.

It was believed that harmonic corrections were unnecessary; therefore a value for γ was determined in a similar manner using the end corrections only.

D. Determination of γ by Median-flux Levels

Inverse relaxation length was also determined by using the median-flux level. Uncorrected median-flux levels were used in place of foil activities in the equation $A = Ce^{-\gamma z}$. A procedure was followed as explained in the preceding section to obtain a value for γ. Values were determined by using only the end-correction factors.

E. Determination of Amplitude Ratio

Basically, the need of the amplitude ratio was to determine if the amplitude of the neutron sine wave varied with

the frequency of the source oscillation. To eliminate any "built-in" variation due to the equipment, the calibration runs next to the oscillator unit were used as the basis for determining the amplitude ratios. The amplitude ratio was defined as the amplitude of the wave obtained for a particular position and speed divided by the calibration-run amplitude at the same speed. Both values of amplitude were obtained from the plots of the data, and to standardize the results, all amplitudes were placed on a one-minute basis.

After the amplitude ratios were obtained from the data, an end-correction factor was applied. From the iterative process explained previously, a value for the end-correction factor was obtained. No end-correction factors were applied to the calibration runs. The end-correction factors were divided into the amplitudes obtained in the hole positions, and it was found that factors were significant only in the top two holes.

There is a definite difference between the theoretical amplitude ratio obtained from Equation 31 and the amplitude ratio obtained from the experiment. Theoretical amplitude ratio was defined as the ratio of amplitude of the observed run divided by that of an infinitely slow run, whereas the experimentally-determined amplitude ratio is the amplitude of the observed run divided by a calibration run. Therefore, numerical values of the two ratios will not agree, but they

will agree in showing any change in amplitude ratio with frequency.

F. Determination of Median-flux Level

The median-flux level is the average flux at a particular hole position and oscillator frequency. From the plots of original data, the amplitude and the lowest value of count rate found in the graph were obtained. The median-flux level was then taken as half the amplitude added to the lowest count rate. End-correction factors were applied to the amplitudes for the top two holes.

VII. RESULTS

The original data for all runs completed including the calibration is given in Tables 5 through 13 in the Appendix. Figure 5 shows a representative plot of original data at a frequency of 2.51 radians/second for all hole positions and calibration.

Phase angle was determined for each run and the results are as given in Table 1. All the calibration runs proved that there is no "built in" phase angle in the equipment. No phase angle is observed in any hole position above 0.63 radians/second. Approximately a 20-degree phase angle is found to exist in all five hole positions at 0.63 radians/second. For the only hole position investigated, number two, a 30-degree phase angle is found at 0.42 radians/second. Verification of the phase angles in hole two up through 4.19 radians/second was obtained by use of the 10-degree cam. No change of phase angle is observed in proceeding to higher positions while taking measurements at the same oscillator frequency.

Amplitude ratios were obtained and the results are as given in Table 2. Figure 6 is a plot of measured amplitude ratio versus oscillator frequency for hole positions one, three and five. Amplitude ratios do not show a definite trend with frequency, but do remain approximately constant

Table 1. Phase angle (degrees)

Frequency radians/second	Hole position						Calibration
	One	Two	Two[a]	Three	Four	Five	
0.42	--	30	30	--	--	--	0
0.63	20	20	20	20	20	20	0
1.05	0	0	0	0	0	0	0
1.68	0	0	0	0	0	0	0
2.51	0	0	0	0	0	0	0
4.19	0	0	0	0	0	0	0
6.28	0	0	--	0	--	--	0
7.33	0	0	--	--	--	--	0
9.42	0	0	--	--	--	--	0
12.55	0	0	--	--	--	--	0
18.85	0	--	--	--	--	--	0

[a]Runs accomplished with 10-dgree cam.

Table 2. Amplitude ratio

Frequency radians/second	Hole position				
	One	Two	Three	Four	Five
0.63	0.0710	0.0330	0.0128	0.00610	0.00418
1.05	0.0678	0.0440	0.0139	0.00663	0.00279
1.68	0.0780	0.0248	0.0083	0.00450	0.00216
2.51	0.0810	0.0180	0.0090	0.00492	0.00274
4.19	0.0690	0.0315	0.0109	0.00454	0.00252
6.28	0.0550	0.0259	0.0083	--	--
7.33	0.0530	--	--	--	--
9.42	0.0678	0.0144	--	--	--
12.55	0.0678	0.0218	--	--	--
18.85	0.0718	--	--	--	--

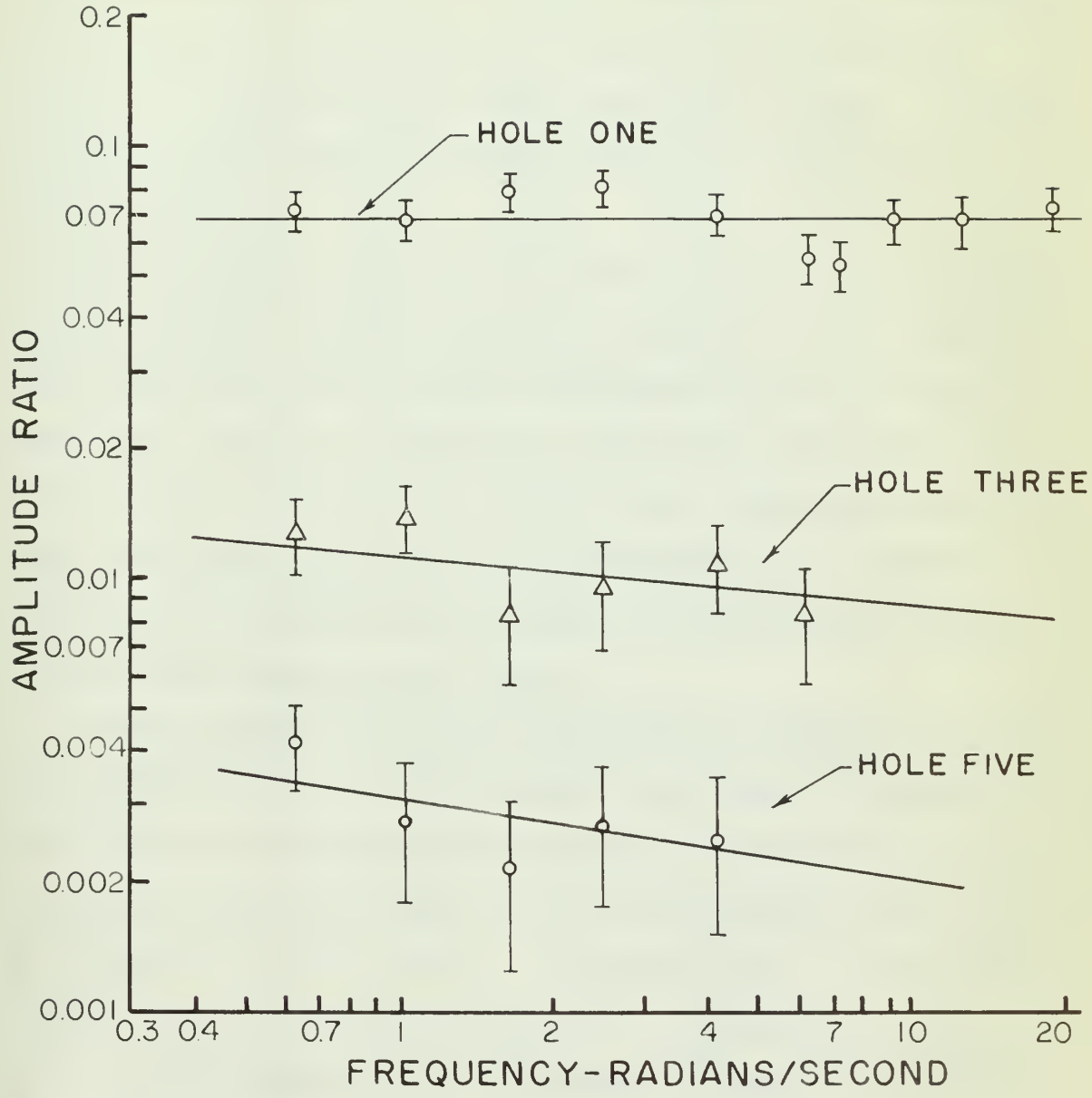

Figure 6. Amplitude ratio vs. frequency

at each hole position. A high coefficient of variation is evident for values above hole one.

Amplitude ratios were also plotted against vertical distance in the assembly. The five frequencies investigated in all five hole positions are represented on this plot, Figure 7. The line slopes drawn correspond to the γ values obtained by the method of least squares for the set of points used.

A median-flux level for each hole position and frequency was determined. Table 3 gives the results of this computation, which also includes the calibration runs. To demonstrate the change in median-flux level with oscillator frequency a plot of these two variables was constructed for the first three hole positions and calibration run. Figure 8 shows that the slopes on logarithmic paper of these lines for the four positions are equal.

Table 4 gives the various values of γ obtained by using the amplitude ratios. Uncorrected values gave an average of 0.0710 inches^{-1}; end-and-harmonic-corrected values gave an average of 0.0631 inches^{-1}, and end-corrected values gave an average of 0.0702 inches^{-1}. End-corrected γ values were plotted versus frequency in Figure 9. Values for γ are approximately constant with frequency. Large coefficients of variation are noted for all the γ values plotted in Figure 9.

Table 3. Median-flux level (total counts)

Frequency radians/second	Hole position					Calibration
	One (2 min.)	Two (2 min.)	Three (3 min.)	Four (4 min.)	Five (5 min.)	(1 min.)
0.63	11,534	5,410	3,585	2,105	1,150	13,585
1.05	11,275	5,635	3,730	2,115	1,265	13,425
1.68	11,350	5,270	3,473	1,998	1,085	13,245
2.51	11,150	5,315	3,590	2,098	1,183	12,947
4.19	10,857	5,113	3,450	2,180	1,098	12,730
6.28	10,980	5,100	3,500	--	--	12,536
7.33	10,634	--	--	--	--	12,495
9.42	10,600	5,078	--	--	--	12,339
12.55	10,490	4,830	--	--	--	12,264
18.85	10,400	--	--	--	--	11,935

Table 4. Inverse-relaxation length $(\text{inches})^{-1}$

Method of computation	Frequency-radians/second					Average
	0.63	1.05	1.68	2.51	4.19	
No corrections	0.0642	0.0714	0.0764	0.0690	0.0739	0.0710
End corrections	0.0640	0.0704	0.0759	0.0676	0.0729	0.0702
End and harmonic corrections	0.0582	0.0638	0.0690	0.0626	0.0664	0.0631

Figure 7. Amplitude ratio vs. vertical distance

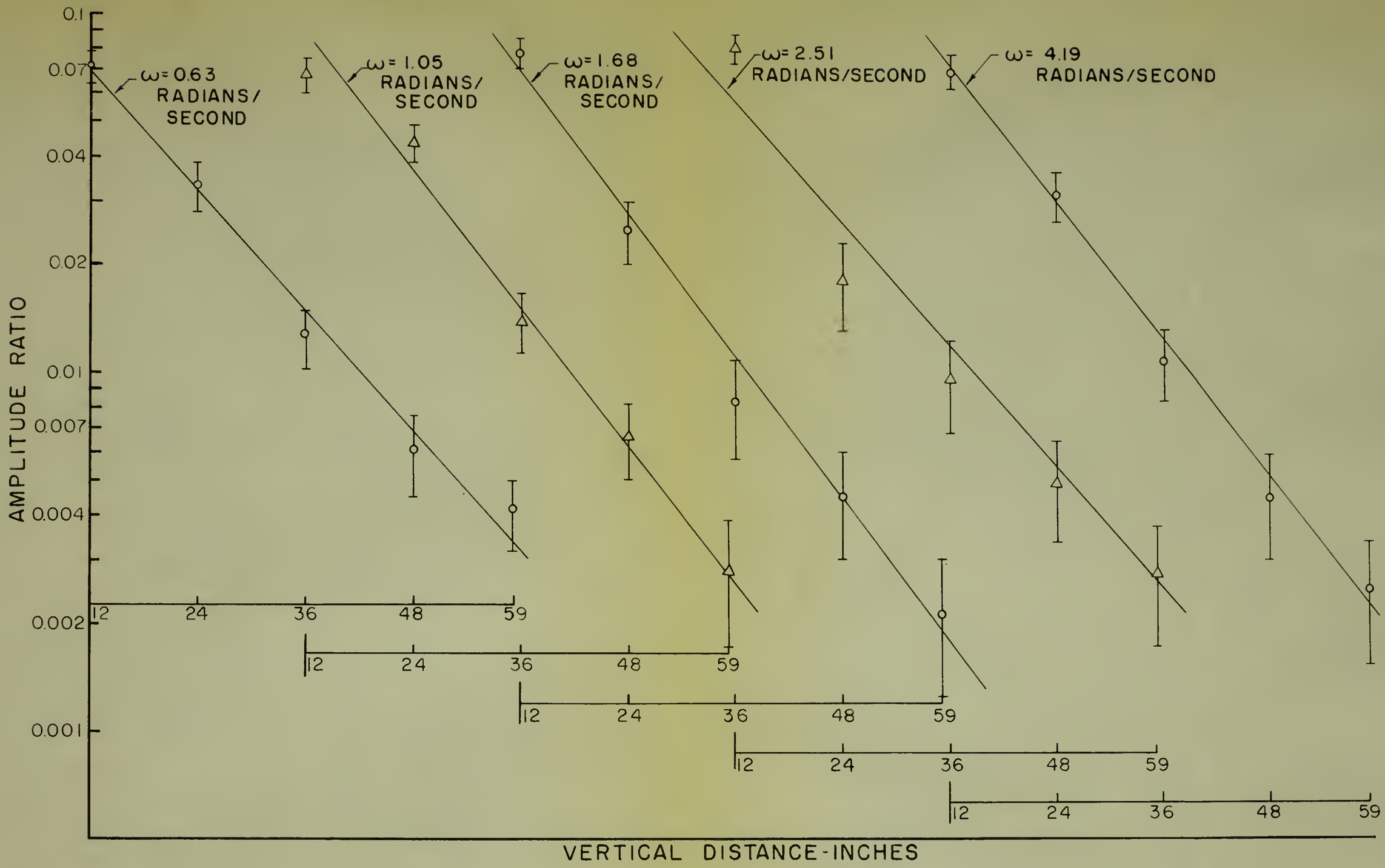
0.1
0.07
0.04
0.02
0.01
0.007
0.004
0.002
0.001
AMPLITUDE RATIO
ω= 0.63 RADIANS/ SECOND
ω= 1.05 RADIANS/ SECOND
ω= 1.68 RADIANS/ SECOND
ω= 2.51 RADIANS/SECOND
ω= 4.19 RADIANS/SECOND
12
24
36
48
59
VERTICAL DISTANCE-INCHES

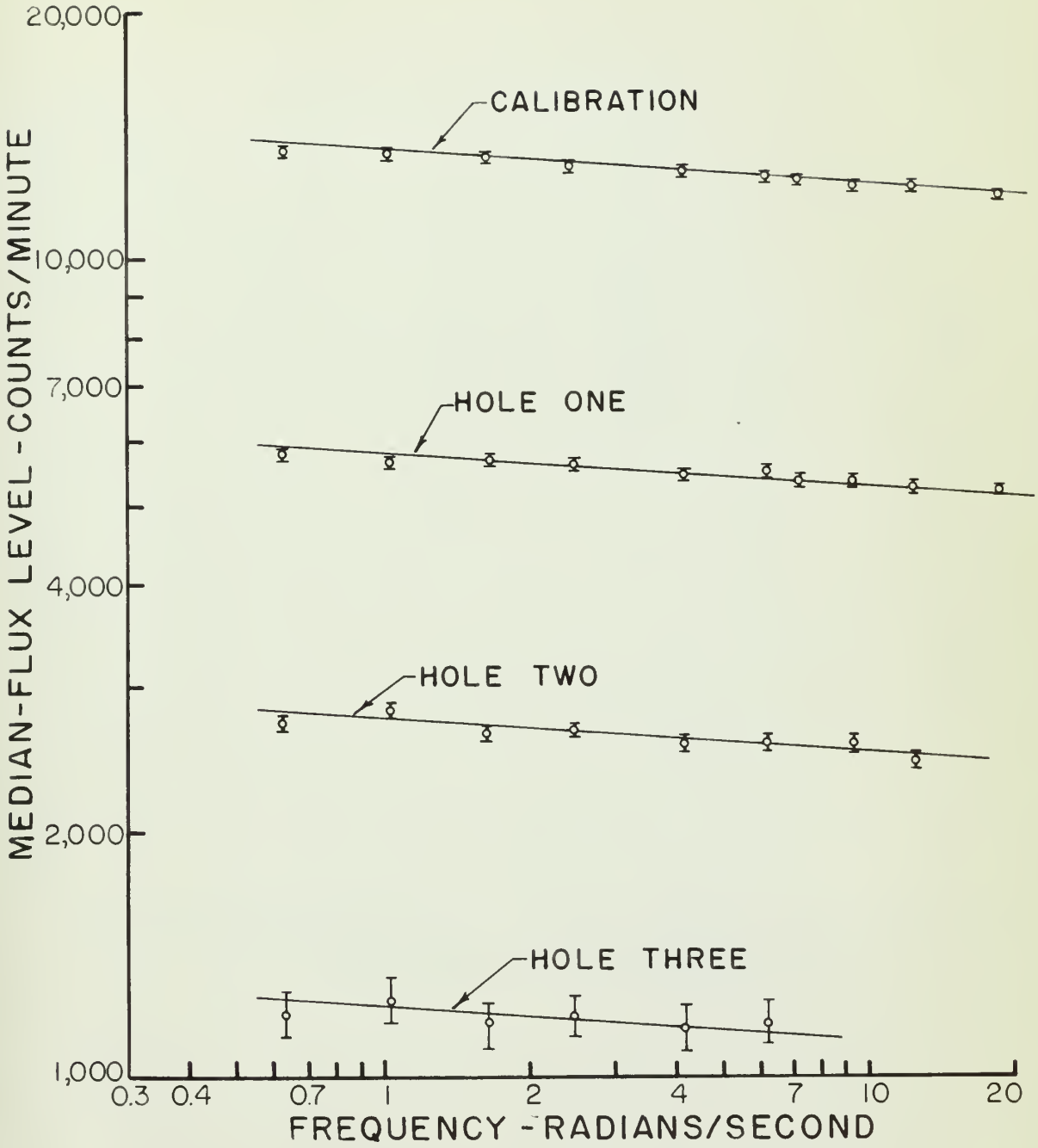

Figure 8. Median-flux level vs. frequency

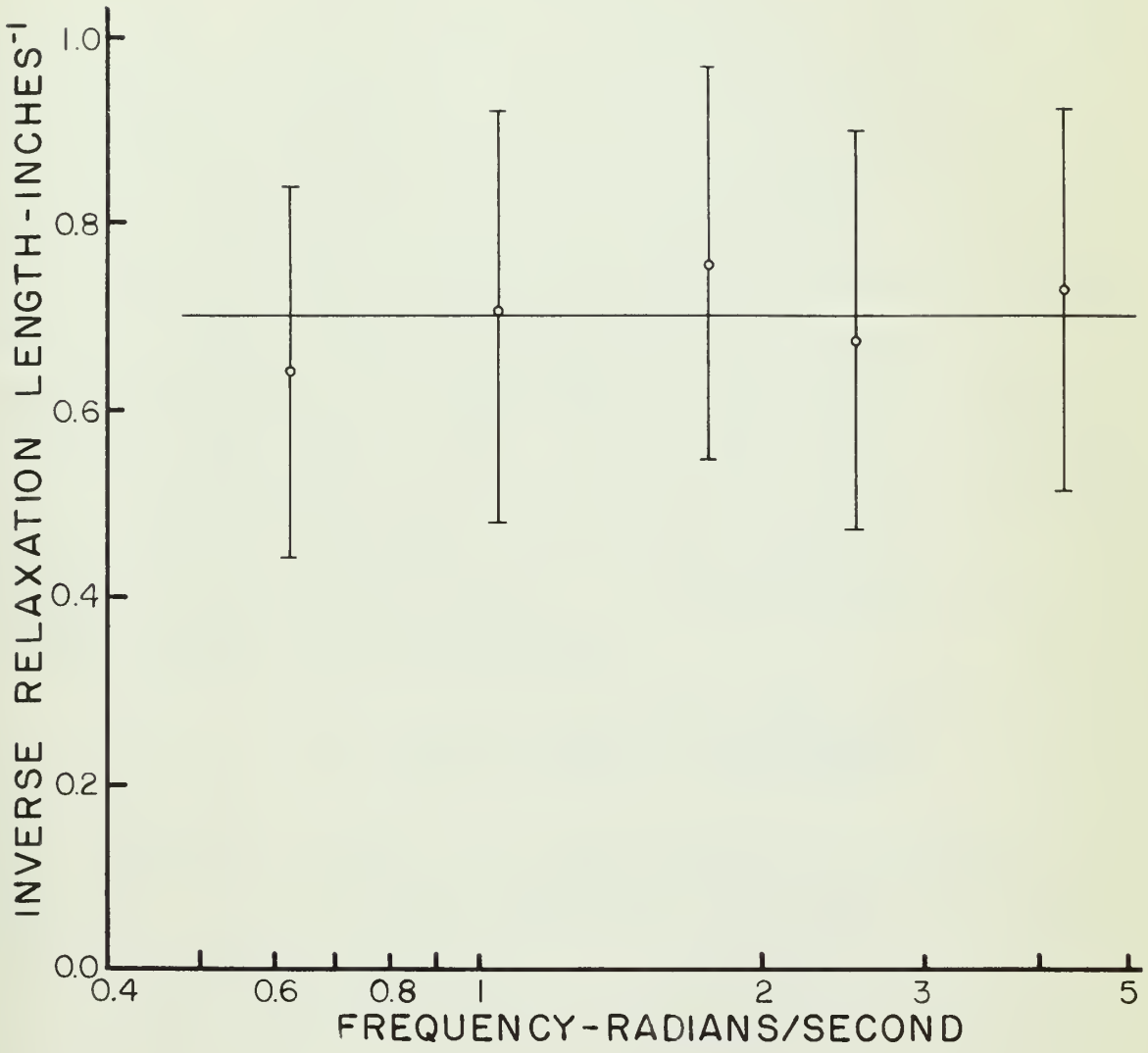

Figure 9. Inverse relaxation length vs. frequency

A value for γ of 0.0681 inches^{-1} was obtained by using the method of median-flux levels.

VIII. DISCUSSION OF RESULTS

It was the original belief that a phase angle would be observed at any oscillator frequency above 0.6 radians/second (13, p. 33). After a series of runs had been completed, this was found not to be true. Previously, the values of k and ℓ had not been known for the assembly used, and had to be assumed. This led to the erroneous prediction.

The theoretical analysis was performed using one average group of delayed neutrons. Figures 10 and 11 show the theoretical phase angle and amplitude ratio respectively as determined from Equation 31. A value for k of 0.53 was used.* With f equal to 0.87 (9, p. 56), and B^2 equal to 70 x 10^{-6} cm^2 (9, p. 57b) a value of ℓ was determined to be 0.00098 seconds from the equations

$$L^2 = L_g^2(1-f) \text{ and } \ell = \frac{\ell_o}{1 + L^2B^2}$$

and an assumed value of $\ell_o = 0.001$ seconds. The total fraction β of the delayed neutrons was set equal to 0.0064 (7) with a corresponding value of λ equal to 0.08 $seconds^{-1}$.

It can readily be seen from Figure 10 that a phase angle would not be observed in the assembly until an oscillator frequency of 40 radians/second is reached. A phase angle

---

*Beck, D. M., Ames, Iowa. Data from partially completed M. S. Thesis. Private communication. 1959.

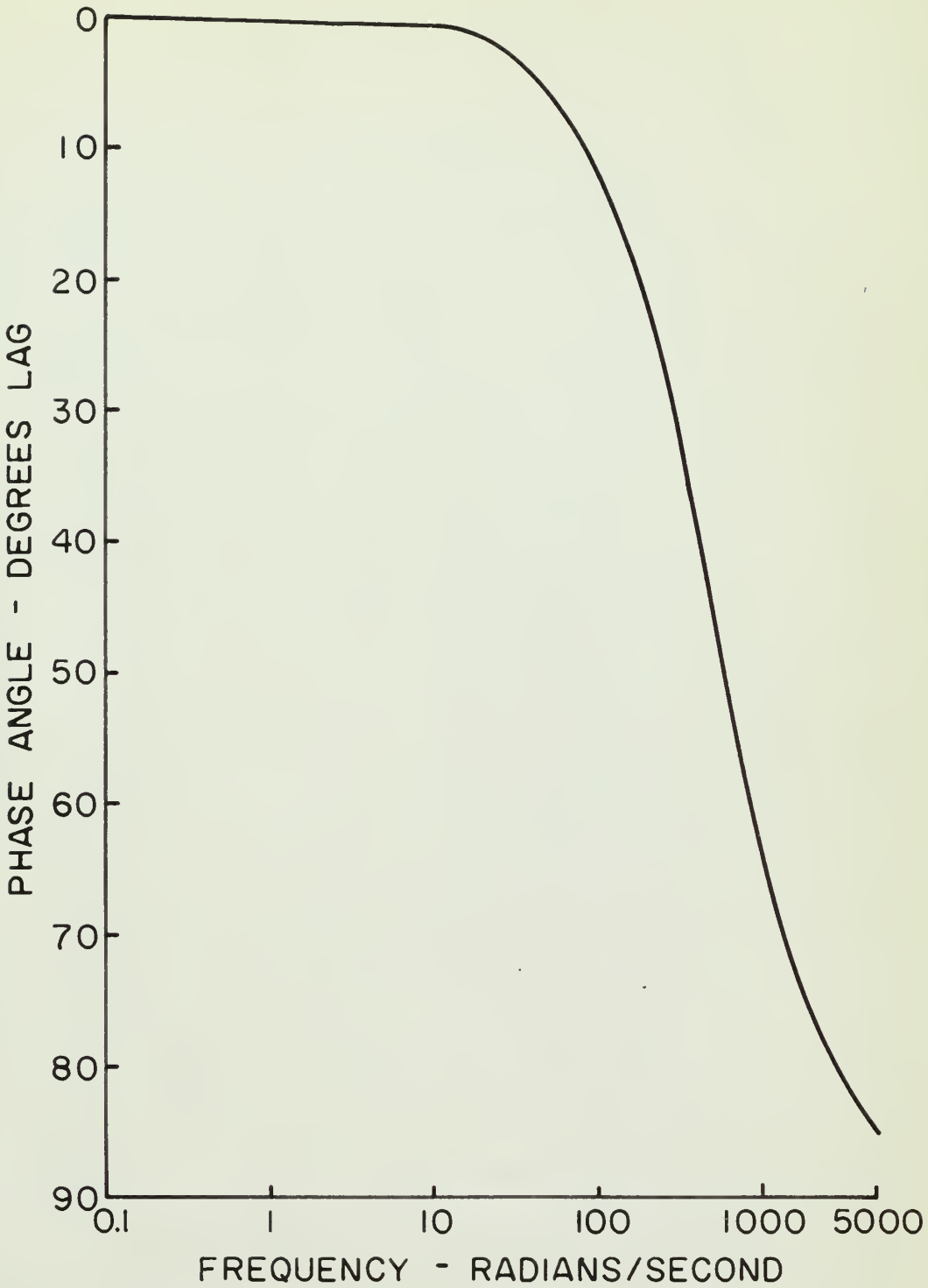

Figure 10. Theoretical phase angle vs. frequency

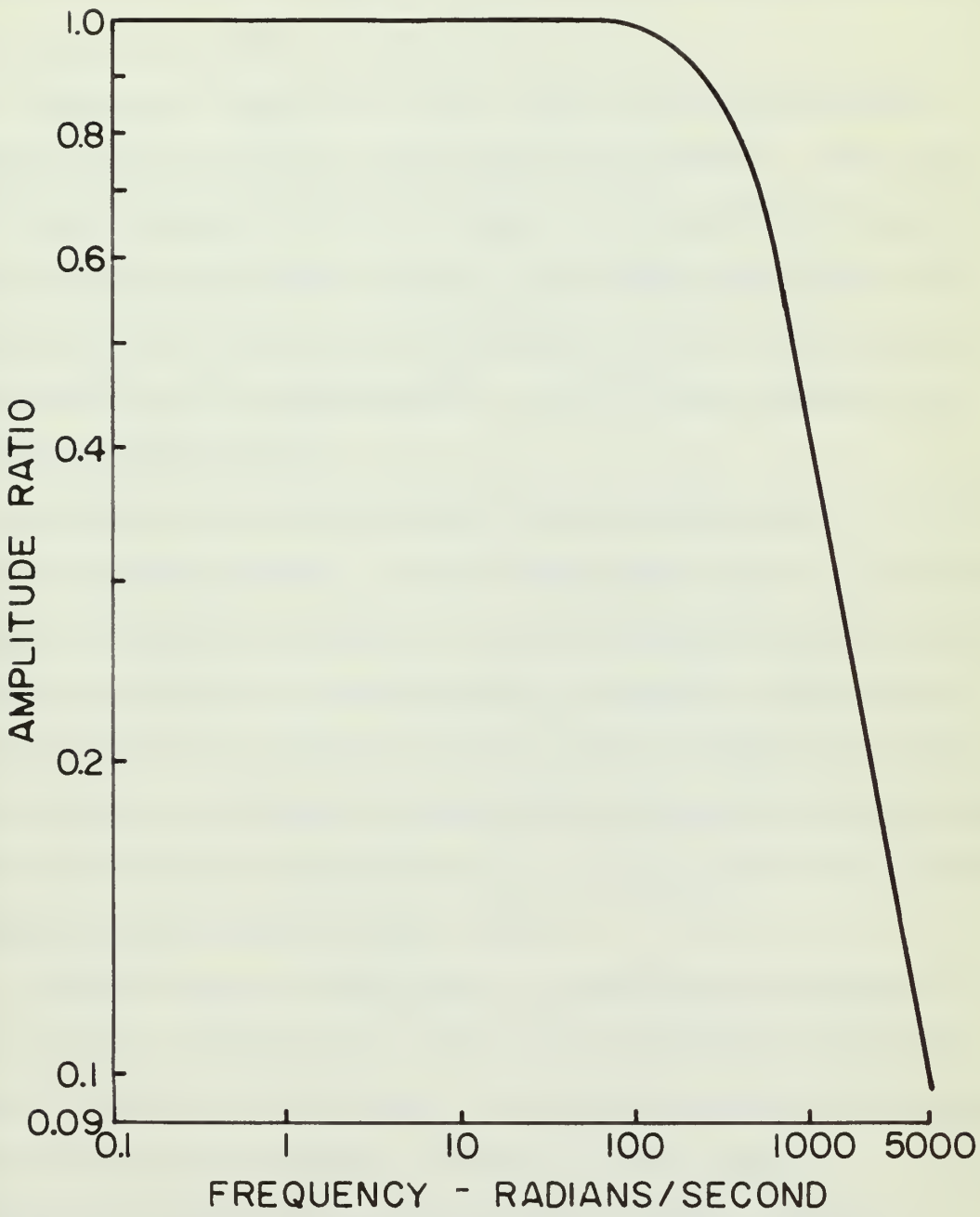

Figure 11. Theoretical amplitude ratio vs. frequency

does not appear for this investigation until very high frequencies because the value of k is low. If k were 0.9 a phase angle would be observed at a frequency of 20 radians/second. The overall shape of the theoretical curve remains the same with varying values of k.

Runs were completed to the lower and upper frequency limits of the oscillator and counting equipment. The upper limit (19 radians/second) is short of the required frequency for an observable phase angle. In complete agreement with theory, no phase angle was observed in any of the hole positions above 0.63 radians/second. Use of the 10-degree cam verified these results.

Readings were taken in all hole positions for a frequency of 0.63 radians/second. A consistent phase angle of approximately 20 degrees is found. At 0.42 radians/second the phase angle in hole two is approximately 30 degrees. The theory advanced does not predict a phase angle at these low values of frequency. Further investigations were not conducted into this low frequency range since the equipment did not provide adequate speed control below 4 RPM.

Theory makes no distinction of position in relation to phase angle; therefore the phase angle should be identical in all areas of the assembly. No change in phase angle with hole position was observed during the investigation. Surveys were taken only up the center of the assembly so the

proof of the constancy of phase angle is limited to this condition. With the method of source forcing used it is believed that some large variations would be found at the edge of the assembly near the base. Simply noting that the pattern position facing these extreme positions will vary as much as 45 degrees from the recorded position indicates the physical reason for the nonconformance.

As shown in Figure 5, the curve of the neutron flux measured at the various hole positions is shown to be sinusoidal. Scatter of points increases as higher hole positions are investigated. The range of frequency for usable data narrows as measurements are taken higher in the assembly. Statistical variations, and inaccuracies in the detector and scaler distort the counts received. Due to the already small amplitude of the sine wave, any distortions cause a scattering of points that make the readings unusable. This situation is aggravated by higher frequencies. As the oscillator frequency increases, the neutron waves are propagated quite close together. Any disturbance or irregularity in the entire assembly or counting system will cause an incorrect measurement to be taken. For example, a measurement is to be taken at a specified oscillator-unit degree. A small disturbance or irregularity will cause the neutron wave to be delayed in reaching the detector. At a high frequency this delay is significant since the portion

of the sine wave actually surveyed may be 30 to 40 degrees removed from the portion desired.

As shown in Figure 5, the standard deviation at hole one is reasonable and acceptable. However as readings are taken at higher positions in the assembly the coefficient of variation caused by standard deviation increases even though longer counting times are allowed. This is caused by lower count rates due to the exponential attenuation of the thermal-neutron flux. An average coefficient of variation for all the runs completed ranges from one to three percent in going from hole one to five. It is seen then that to obtain coefficients of variation of less than two percent at the higher hole positions, very long counting times are needed, in the order of 10 minutes at hole five.

Amplitude ratios were determined and are given in Table 2. These amplitude ratios for holes one, three and five were plotted against frequency in Figure 6. A least squares analysis was applied to the data for holes three and five, and it was found that the line joining hole-three data had a slope of -0.184 ± 0.225, and the line joining hole-five data had a slope of -0.231 ± 0.344. This indicates that a horizontal line representing a constant value of amplitude ratio with frequency lies easily within the standard deviation for the slopes found for both holes. It is believed that the amplitude-ratio values are approximately constant as predicted by Figure 11 and that

the slopes shown on Figure 6 are caused by the high standard deviation rather than variance of amplitude ratio with frequency.

Figure 11 has the overall shape that the amplitude ratio versus frequency would have for any value of k. For a k greater than 0.53, an amplitude ratio less than one would be noted at frequencies less than indicated on Figure 11.

Scatter of the points in Figure 6 is due to a very high coefficient of variation. As was mentioned previously, some scatter of points is present at all positions especially in the higher hole positions at higher frequencies. Error occurs when fairing in the curves to fit the data. A very significant error occurs when the standard deviation of the points is large compared to the amplitude. For example, at hole three a standard deviation of approximately 60 counts is found; however an amplitude of only 300 counts exists. Coefficient of variation caused by standard deviation of the amplitude is then approximately 20 percent. The condition is exaggerated at higher hole positions such that a 36 to 42 percent coefficient of variation in hole five is noted. Significant errors appear for the amplitude ratios above hole one. Considerably longer counting times are needed at all higher hole positions to give satisfactory results. A counting time of approximately 10 minutes would give a 13 percent coefficient of variation for hole four.

Even though the coefficients of variation for the amplitude ratios are quite high, the results are believed to be sufficiently accurate and repetitive to support the conclusions drawn.

Values of the median-flux level are given in Table 3 and the plot of level versus frequency is shown as Figure 8. Deviation was so slight in holes four and five that they were not included in the figure.

The transfer-function development does not predict a decrease in the median flux, yet all four curves show that median-flux level does decline as frequency increases. Slopes on the logarithmic plot (Figure 8) of all four lines are found to be equal. If each line is represented by the equation $\phi = K\omega^n$, where K is a constant and n is the slope of the line, then the rate of neutron-flux decline with frequency is

$$\frac{d\phi}{d\omega} = \frac{Kn\omega^n}{\omega} = \frac{n\phi}{\omega} .$$

The relative rate of decline is

$$\frac{\frac{d\phi}{d\omega}}{\phi} = \frac{n}{\omega} .$$

With identical values of n, and the same values of ω, each hole position has the same relative rate of decline. The decline is therefore not a function of the assembly.

The decline is attributed to either the method of source forcing or to the counting equipment. No logical reason can be advanced for the unit itself to cause the decline, but the counting equipment could easily have caused this unpredicted result. The number of activations of the preset-count relay is in proportion to the frequency. A small relay lag would then become important at higher frequencies and significantly reduce the amount of time the scaler was counting. Furthermore, investigation shows that the reduction of thermal neutrons and fast neutrons counted is in proportion to their total counts. The deviation from theory is therefore said to be a mechanical irregularity of the counting equipment rather than a function of the assembly.

Amplitude ratios were not affected by the decline of counts with frequency since the calibration runs were used as the denominator of the ratio.

When plotted on semi-log paper, amplitude ratio versus vertical distance gives a reasonably straight line. Figure 7 shows the results for frequencies from 0.63 to 4.19 radians/second. As noted previously, the large coefficients of variation of data for the higher hole positions result in some scatter of the amplitude ratios. It is seen, however, that the points nearly all lie close to the straight lines indicating that the points can be considered reliable. Standard deviation of the amplitude ratios is indicated on the figure.

Values for inverse relaxation length, γ , were computed for the frequencies. These values obtained by an iterative process are listed in Table 4, and it is found that values range from 0.0582 to 0.0759 inches^{-1}. A value for γ was found without using either the end or harmonic corrections; the average value was 0.0710 inches^{-1}. When both corrections were applied, an average value of 0.0631 inches^{-1} was found. It is believed however that the higher harmonics have been greatly lessened with this particular arrangement of sources in the oscillator. The sources are placed in a line and are surrounded by three inches of paraffin which thermalizes many of the neutrons produced. The paraffin, lined sources, and two water-filled tanks in the outermost pedestal spaces help to scatter the neutrons more uniformly beneath the base, so that a plane source of thermal neutrons is approximated. Dopchie, Leonard, Neve de Mevergnies and Tavernier (3) showed in their work with an exponential assembly that distributing four sources in a square form reduced the harmonic-correction term to 5 percent or one-fourth the correction needed when the sources were placed together.

With application of just the end corrections an average value for γ of 0.0702 inches^{-1} was determined. Hayes (8, p. 27) found by the method of foil irradiation that the assembly in this configuration had a γ of 0.0705 inches^{-1}. Harmonic-correction factors would appear then not to be

needed, or if used the full correction should not be applied. Line slopes on Figure 7 are the γ values determined by using only the end corrections.

Values of inverse relaxation length obtained by using end corrections only were plotted with frequency on Figure 9. A standard deviation for γ was obtained by using the method of propagation of precision indexes as presented by Worthing and Geffner (17, p. 209) and are indicated on the figure. Large coefficients of variation are again noted for γ. This is due to the high coefficients of variation of the amplitude ratios, especially at the higher hole positions. By using longer counting times the relative standard deviation of the amplitude ratios would be greatly reduced and statistically better values of γ would follow. For example, if an average relative standard deviation of 5 percent were found for the amplitude ratios, then the coefficient of variation for γ in this experiment would decrease by a factor of approximately six.

It is seen from Figure 9 that there is no trend in γ with increasing frequency. A constant value of γ should be found, but due to the high standard deviations values differing slightly from the average of 0.0702 inches^{-1} are noted.

To substantiate the values of γ determined by using amplitude ratios an average value of γ was found by using the median-flux levels. As shown on Figure 12 the values of

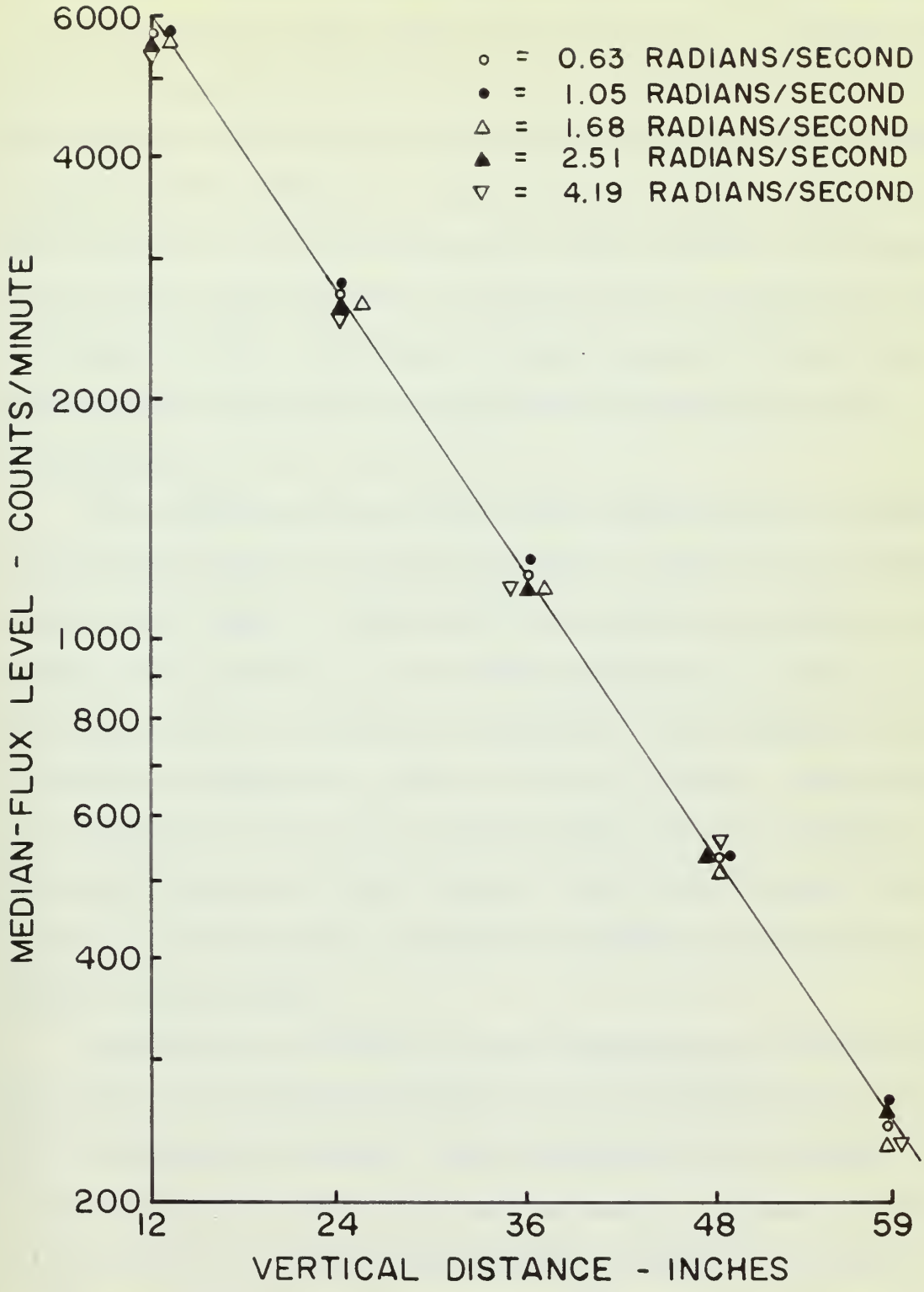

Figure 12. Median-flux level vs. vertical distance

the median flux are grouped close together. An average value was obtained from each group and a value of γ computed from them by using end corrections only. Standard deviation of the average points is approximately the size of the symbols, therefore the value of γ obtained is reliable. From Figure 12 a value of γ was found to be 0.0681 inches^{-1} in comparison to the average value of 0.0702 inches^{-1} computed by using amplitude ratios. Agreement within 3 percent between the two methods indicates the amplitude-ratio method to be acceptable.

The validity of the statements concerning the attenuation length and $1/\gamma$ was investigated. Values used in the computation were $\tau = 350$ cm^2 (16, p. 331), $k_p = k(1 - \beta) = 0.526$, $L^2 = 325$ cm^2, $\ell_o = 0.001$ seconds and $\omega = 20$ radians/second. A value was determined from Equation 32 for attenuation length and found to be 14.8 inches. The inverse of this number is 0.0676 inches^{-1} which agrees favorably with the values of 0.0702 inches^{-1} and 0.0681 inches^{-1} obtained by the methods of amplitude ratios and median-flux levels respectively.

Frequencies utilized in the experiment were small enough to cause the attenuation length to be approximately equal to the relaxation length. From Equation 32 it is noted that a frequency of 20 radians/second produces negligibe change in the value of attenuation length as compared to very low

frequencies. Hence from the previous computations and discussion it appears that the attenuation length and consequently the complex buckling for the frequencies investigated are approximately the same as relaxation length and material buckling. Therefore it would be proper in this case to utilize the values of attenuation length for determining γ. Even with the combination of varying and steady neutron flux, computation of γ by amplitude ratio and median-flux level is feasible since the frequency never is large enough to produce significant changes in γ.

For assemblies with much larger values of k_p, frequencies used in this experiment would produce changes in the attenuation length and give varying values for the complex buckling, therefore the inverse attenuation length would not be equal to the inverse relaxation length.

IX. CONCLUSIONS

A theoretical and experimental investigation into neutron diffusion in the subcritical assembly with sinusoidal source oscillation was conducted at Iowa State College. An oscillator unit produced the sinusoidal source oscillation of the thermal neutrons, while a selective-count device allowed discrete sections of the sine wave to be observed and counted. Neutron-diffusion information was extracted from plots of these counts. Conclusions drawn from the information are that:

1. No phase angle is observed for oscillator frequencies between 0.63 and 18.85 radians/second. This is in agreement with theory.

2. An unpredicted phase angle of 20 degrees is observed at a frequency of 0.42 radians/second and an angle of 30 degrees at 0.63 radians/second.

3. There is no phase-angle change at higher hole positions on the centerline of the assembly at the same oscillator frequency, which ranged from 0.63 radians/second to 6.28 radians/second. This is in agreement with theory.

4. Amplitude ratios for a given hole are approximately constant for varying frequencies from 0.63 radians/second to 6.28 radians/second. This is in agreement with theory.

5. The median-flux level decreases as frequency increases. Mechanical operation of the counting equipment

causes this change rather than any assembly peculiarities or characteristics. A change in level is not predicted by theory.

6. The oscillator unit thermalizes enough neutrons to give satisfactory readings up through hole five up to 4.19 radians/second. Any frequency readings above 12.55 radians/second are confined to hole one.

7. An inverse relaxation length of 0.0702 inches^{-1} was determined by using amplitude ratios.

8. An inverse relaxation length of 0.0681 inches^{-1} was determined by using median-flux levels.

9. The attenuation length of the neutron wave is equal to a constant value of $1/\gamma$ for the assembly and frequencies investigated.

10. Longer count times are needed to reduce coefficients of variation in the amplitude ratios. In all other respects the experimental equipment and procedure will yield satisfactory results within certain frequency limits for phase angle, amplitude ratio and inverse relaxation length.

X. SUGGESTIONS FOR FURTHER STUDY

From a review of the literature it is obvious that neutron diffusion in a subcritical assembly with sinusoidal source oscillation has not been fully investigated.

The equipment used in this experiment can be improved in several ways. Another speed reducer could be introduced to allow speeds below 4 RPM to be utilized. The cam could be replaced by a phototube device that would trigger the scaler at the higher frequencies. An automatic revolution counter would be necessary to measure the frequency at the higher speeds. A gating circuit would be more desirable to interrupt pulses going to the scaler than using the preset-time relay which is burdened at high frequencies. Still another possibility might be to use an ionization chamber connected to a sensitive electrometer. The wave produced by a recorder connected to the electrometer could then be analyzed for data desired.

In this experiment, only the center of the assembly was investigated. Measurements could be taken throughout the assembly to see if the thermal-neutron flux behaved in the same manner as the flux produced by a steady source. Further theoretical and experimental work with neutron waves could be accomplished with an investigation into the change in prompt buckling by source forcing. Speeds considerably below and

above those investigated here could also be utilized to expand the experimental verification of the theoretical transfer function. The above suggestions could be expanded greatly by changing the lattice in the assembly and repeating the particular investigation. Voids and absorbers could also be placed in the assembly to observe the effect of them upon the neutron wave.

XI. LITERATURE CITED

1. Axtmann, R. C., Dessauer, G. and Parkinson, T. F. Reactivity measurements in a subcritical pile. U. S. Atomic Energy Commission Report DF-48 [Du Pont de Nemours (E. I.) and Co., Wilmington, Del.] November 1955.

2. Dana, F. C. and Hillyard, L. R. Engineering problems manual. New York, N. Y., McGraw-Hill Book Co., Inc. 1947.

3. Dopchie, H., Leonard, F., Neve de Mevergnies, M. and Tavernier, G. Conducting an exponential experiment with a natural - U graphite lattice. Nucleonics 14: 57-60. March 1956.

4. Franz, J. P. Pile transfer functions. U. S. Atomic Energy Commission Report AECD-3260. [Technical Information Service, AEC]. July 18, 1949.

5. Glasstone, S. Principles of nuclear reactor engineering. Princeton, N. J., D. Van Nostrand Co., Inc. 1955.

6. _____ and Edlund, M. C. The elements of nuclear reactor theory. Princeton, N. J., D. Van Nostrand Co., Inc. 1952.

7. Hadley, J. W. Speech delivered to the Iowa State College American Nuclear Society Student Chapter. Univ. of Calif., Livermore, Calif., Author. January 15, 1959.

8. Hayes, J. T. Flux distribution in a unit cell of a uranium graphite subcritical assembly. Unpublished M.S. Thesis. Ames, Iowa, Iowa State College Library. 1958.

9. Hoganson, J. H. Operating characteristics of a uranium graphite subcritical assembly with coolant simulation. M.S. Thesis. Ames, Iowa, Iowa State College Library. 1957.

10. Martin, D. H. Correction factors for measurements with cadmium covered foils. U. S. Atomic Energy Commission Report NAA-SR-1076 [North American Aviation, Inc., Downey, Calif.]. October 15, 1954.

11. Murray, R. L. Nuclear reactor physics. Englewood Cliffs, N. J., Prentice-Hall, Inc. 1957.

12. Owens, J. I., Jr., Crever, F. E. and Pigott, J. H. A proposed automatic control system for the Schenectady reactor. U. S. Atomic Energy Commission Report AECD-4209 [Technical Information Service, AEC]. March 29, 1949.

13. Ricci, W. J. Transfer function of a uranium-graphite subcritical assembly. Unpublished M.S. Thesis. Ames, Iowa, Iowa State College Library. 1958.

14. Soodak, H. Pile kinetics. In Goodman, C., ed. The science and engineering of nuclear power. Vol. 2, pp. 89-102. Cambridge, Mass., Addison-Wesley Press. 1949.

15. Weinberg, A. M. and Schweinler, H. C. Theory of oscillating absorber in a chain reactor. Physical Review 74: 851-863. 1948.

16. _____ and Wigner, E. P. The physical theory of neutron chain reactors. Chicago, Ill., The University of Chicago Press. 1958.

17. Worthing, A. G. and Geffner, J. Treatment of experimental data. New York, N. Y., John Wiley and Sons, Inc. 1955.

XII. ACKNOWLEDGMENTS

The author wishes to thank Dr. Robert E. Uhrig for his original suggestion of this project; and especially for his tireless assistance and sincere interest in all phases encountered both in this specific project and in the course work here at Iowa State College. Many thanks are due Dr. Glenn Murphy for his guidance and encouragement given to the author during this course of study.

This thesis culminates three years of study under the auspices of the U. S. Navy in its postgraduate training program. The author wishes to express his appreciation to the United States Naval Postgraduate School for making this year at Iowa State College possible.

XIII. APPENDIX

Table 5. Original data at 0.63 radians/second (total number of counts)

Oscillator position	Hole position				
degrees	One (3 min.)	Two (3 min.)	Three (3 min.)	Four (4 min.)	Five (5 min.)
0	17,900	8,623	3,794	2,254	1,234
30	18,511	8,711	3,768	2,220	1,257
60	18,310	8,600	3,660	2,170	1,281
90	18,056	8,224	3,640	2,105	1,199
120	17,276	8,189	3,650	2,102	1,134
150	16,306	7,847	3,522	2,031	1,074
180	16,026	7,708	3,374	1,977	1,042
210	15,995	7,528	3,368	1,984	1,100
240	16,248	7,745	3,484	2,016	1,077
270	17,009	7,998	3,491	2,036	1,086
300	16,971	7,825	3,496	2,040	1,103
330	17,747	8,058	3,685	2,118	1,164

Table 6. Original data at 1.05 radians/second (total number of counts)

Oscillator position	Hole position				
degrees	One (2 min.)	Two (2 min.)	Three (3 min.)	Four (4 min.)	Five (5 min.)
0	11,950	6,342	3,963	2,248	1,297
30	11,917	6,036	3,937	2,291	1,370
60	11,681	5,721	3,716	2,165	1,309
90	11,471	5,386	3,715	2,215	1,282
120	11,017	5,351	3,701	2,193	1,201
150	10,749	5,230	3,565	2,019	1,209
180	10,500	5,223	3,498	1,968	1,200
210	10,455	5,198	3,582	1,984	1,242
240	11,207	5,233	3,660	2,034	1,238
270	11,777	5,287	3,554	2,111	1,268
300	11,218	5,478	3,769	2,206	1,229
330	11,373	5,788	3,879	2,239	1,249

Table 7. Original data at 1.68 radians/second (total number of counts)

Oscillator position	Hole position				
degrees	One (2 min.)	Two (2 min.)	Three (3 min.)	Four (4 min.)	Five (5 min.)
0	12,179	5,510	3,563	2,082	1,110
30	12,081	5,513	3,479	2,090	1,151
60	11,852	5,426	3,448	2,154	1,096
90	11,471	5,283	3,540	2,067	1,099
120	11,065	5,282	3,444	1,959	1,113
150	10,598	5,114	3,460	1,932	1,084
180	10,625	4,982	3,310	1,924	1,076
210	10,571	5,000	3,439	1,894	1,035
240	10,946	5,214	3,369	1,951	1,028
270	11,291	5,191	3,525	1,981	1,039
300	11,665	5,189	3,479	1,956	1,118
330	12,257	5,234	3,499	1,982	1,131

Table 8. Original data at 2.51 radians/second (total number of counts)

Oscillator position	Hole position				
degrees	One (2 min.)	Two (2 min.)	Three (3 min.)	Four (4 min.)	Five (5 min.)
0	12,027	5,481	3,656	2,196	1,235
30	11,807	5,407	3,641	2,110	1,221
60	11,729	5,428	3,588	2,177	1,212
90	11,224	5,354	3,589	2,048	1,182
120	10,765	5,381	3,522	2,034	1,141
150	10,467	5,197	3,448	2,000	1,151
180	10,315	5,153	3,394	2,002	1,110
210	10,379	5,252	3,453	1,973	1,124
240	10,814	5,298	3,526	2,092	1,149
270	11,421	5,383	3,601	2,150	1,185
300	11,515	5,424	3,584	2,136	1,186
330	11,891	5,436	3,673	2,194	1,169

Table 9. Original data at 4.19 radians/second (total number of counts)

Oscillator position	Hole position				
degrees	One (2 min.)	Two (2 min.)	Three (2 min.)	Four (4 min.)	Five (5 min.)
0	11,590	5,316	2,417	2,073	1,124
30	11,585	5,408	2,396	2,053	1,145
60	11,376	5,307	2,319	1,974	1,142
90	10,895	5,236	2,337	1,967	1,126
120	10,448	5,326	2,279	1,989	1,063
150	10,209	4,975	2,221	1,944	1,072
180	10,137	4,857	2,183	1,884	1,032
210	10,269	4,896	2,241	1,949	1,087
240	10,680	4,827	2,252	1,952	1,127
270	11,423	4,992	2,266	2,001	1,108
300	11,246	5,222	2,309	1,994	1,113
330	11,360	5,406	2,365	2,103	1,126

Table 10. Original data at 6.28 radians/second (total number of counts)

Oscillator position	Hole position		
degrees	One (1 min.)	Two (1 min.)	Three (3 min.)
0	5,843	3,211	4,086
30	5,708	3,241	4,051
60	5,680	3,156	4,012
90	--	3,120	3,908
120	5,641	3,013	3,857
150	5,337	2,989	3,823
180	5,271	2,981	3,820
210	5,334	3,050	3,830
240	5,521	3,129	3,867
270	--	3,130	3,897
300	5,720	3,188	3,990
330	5,735	3,245	4,058

Table 11. Original data at hole position one (total number of counts)

Oscillator position	Radians/second			
degrees	7.33 (3 min.)	9.42 (2 min.)	12.55 (1 min.)	18.85 (1 min.)
0	16,347	11,261	5,580	5,367
30	16,474	11,253	5,452	5,614
60	15,939	10,843	5,414	5,359
90	15,865	10,341	5,354	5,161
120	15,249	10,458	5,067	4,985
150	15,188	9,962	4,894	4,879
180	15,208	9,942	4,901	4,700
210	15,320	10,140	4,929	4,916
240	15,932	10,729	5,148	5,241
270	16,402	10,970	5,218	5,326
300	16,390	11,133	5,508	5,516
330	16,655	11,196	5,605	5,308

Table 12. Original data at hole position two (total number of counts)

Oscillator position	Radians/second			
degrees	7.33 (3 min.)	9.42[a] (2 min.)	9.42[b] (2 min.)	12.55 (1 min.)
0	7,514	5,187	5,182	4,951
30	7,689	5,058	5,197	4,906
60	7,602	5,135	5,069	5,021
90	7,382	5,042	5,058	4,978
120	7,298	4,963	5,110	4,647
150	7,398	4,975	5,111	4,684
180	7,577	4,829	4,966	4,573
210	7,388	4,870	4,972	4,751
240	7,583	4,975	5,163	4,750
270	7,677	5,147	5,239	4,985
300	7,551	5,332	5,261	4,938
330	7,539	5,232	5,270	5,063

[a]First run.

[b]Second run.

Table 13. Original data for calibration (counts/minute)

Oscillator position	Radians/second					
degrees	0.42	0.63	1.05	1.68	2.51	4.19
0	16,658	19,215	18,956	18,700	18,218	18,003
30	17,374	18,291	18,338	18,757	18,269	17,513
60	16,174	17,270	17,366	17,475	17,377	17,016
90	14,729	16,880	16,140	15,585	15,615	14,897
120	13,227	13,609	13,153	12,384	12,576	12,442
150	9,155	9,543	9,701	9,580	9,453	8,957
180	8,049	7,947	7,890	7,790	7,677	7,460
210	8,573	8,878	8,651	8,207	8,371	8,169
240	10,693	11,497	11,333	10,989	10,955	10,726
270	--	14,412	14,657	14,104	13,881	13,591
300	--	17,078	16,562	16,604	16,343	16,223
330	--	18,382	18,198	17,777	17,763	17,149

degrees	6.28	7.33	9.42	12.55	18.85
0	17,894	17,897	17,353	17,542	17,162
30	16,954	17,781	16,959	17,128	16,689
60	15,783	16,361	15,450	15,812	15,848
90	13,244	14,208	12,912	13,748	13,823
120	10,517	11,001	10,019	10,790	10,726
150	7,783	8,505	7,407	8,419	7,923
180	7,171	7,095	6,939	6,986	6,709
210	8,419	7,758	8,401	8,068	8,144
240	11,594	10,659	11,391	10,719	10,844
270	14,907	14,066	14,041	13,698	13,412
300	16,832	16,303	16,077	15,882	15,389
330	17,849	17,642	17,308	16,967	16,353